Sciences approved by the Physiological Society of Japan. All protocols were approved by the Animal Subjects Committee of the National Cardiovascular Center. Adult cats weighing from 2.2 to 4.2 kg were anesthetized via an intraperitoneal injection of pentobarbital sodium (30–35 mg/kg) and ventilated mechanically with room air mixed with oxygen. The depth of anesthesia was maintained with a continuous intravenous infusion of pentobarbital sodium (1–2 $mg \cdot kg^{-1} \cdot h^{-1}$) through a catheter inserted from the right femoral vein. Systemic arterial pressure was monitored from a catheter inserted from the right femoral artery. The vagi were sectioned bilaterally at the neck. The esophageal temperature of the animal, which was measured by a thermometer (CTM-303, TERUMO, Japan), was maintained at around 37°C using a heated pad and a lamp.

With the animal in the lateral position, the left fifth and sixth ribs were resected to expose the heart. A dialysis probe was implanted transversely, using a fine guiding needle, into the anterolateral free wall of the left ventricle perfused by the left anterior descending coronary artery (LAD). Heparin sodium (100 U/kg) was administered intravenously to prevent blood coagulation. At the end of the experiment, the experimental animals were killed with an overdose of pentobarbital sodium. Postmortem examination confirmed that the dialysis probe had been threaded in the middle layer of the left ventricular myocardium. The thickness of the left ventricular free wall was ~7–8 mm, and the semipermeable membrane of the dialysis probe was positioned ~3–4 mm from the epicardial surface.

Dialysis Technique

The materials and properties of the dialysis probe have been described previously (1). Briefly, we designed a transverse dialysis probe. A dialysis fiber of semipermeable membrane (13 mm length, 310 μm OD, 200 μm ID; PAN-1200, 50,000 molecular weight cutoff, Asahi Chemical, Japan) was glued at both ends to polyethylene tubes (25 cm length, 500 μm OD, 200 μm ID). The dialysis probe was perfused at a rate of 2 μl/min with Ringer solution containing a cholinesterase inhibitor eserine (physostigmine, 100 μM). Experimental protocols were started 2 h after the dialysis probe was implanted when the ACh concentration in the dialysate reached a steady state. The ACh concentration in the dialysate was measured by high-performance liquid chromatography with electrochemical detection (Eicom, Kyoto, Japan).

Local administration of a pharmacological agent was carried out through a dialysis probe. That is to say, we added the pharmacological agent to the perfusate and allowed 1 h for a settling time. The pharmacological agent should spread around the semipermeable membrane, thereby affecting the neurotransmitter release in the vicinity of the semipermeable membrane. Because the distribution across the semipermeable membrane is required, based on previous results (33, 34), we used the pharmacological agent at the concentration 10–100 times higher than that required for complete channel blockade in experimental settings in vitro.

Specific Preparation and Protocols

Protocol 1. Bipolar platinum electrodes were attached bilaterally to the cardiac ends of the sectioned vagi at the neck. The nerves and electrodes were covered with warmed mineral oil for insulation. The vagal nerves were stimulated for 15 min (20 Hz, 1 ms, 10 V). We measured the stimulation-induced ACh release in the absence of Ca^{2+} channel blockade (control, $n = 7$) and examined the effects of an L-type Ca^{2+} channel antagonist verapamil (100 μM, $n = 5$), an N-type Ca^{2+} channel antagonist ω-conotoxin GVIA (10 μM, $n = 7$), a P/Q-type Ca^{2+} channel antagonist ω-conotoxin MVIIC (10 μM, $n = 6$), and combined administration of ω-conotoxin GVIA and ω-conotoxin MVIIC (10 μM each, $n = 6$).

Protocol 2. Because a preliminary result from *protocol 1* suggested that local administration of verapamil was ineffective in suppressing stimulation-induced ACh release, we examined the effects of the intravenous administration of verapamil (300 μg/kg, $n = 6$) on stimulation-induced ACh release in vagotomized animals as a supplemental experiment.

Protocol 3. A 60-min LAD occlusion was performed by using a 3-0 silk suture passed around the LAD just distal to the first diagonal branch. We measured the ACh levels during 45–60 min of ischemia in the absence of Ca^{2+} channel blockade (control, $n = 8$) and examined the effects of verapamil (100 μM, $n = 5$), ω-conotoxin GVIA (10 μM, $n = 5$), and ω-conotoxin MVIIC (10 μM, $n = 5$). A previous result indicated that the ischemia-induced ACh release reached the steady state during 45–60 min of ischemia (14). We also examined the effects of three additional agents, a Na^+/Ca^{2+} exchange inhibitor KB-R7943 (10 μM, $n = 5$) (9, 10), an $Ins(1,4,5)P_3$ receptor blocker xestospongin C (500 μM, $n = 6$) (25), and a nonselective cation channel blocker or a cation-selective stretch activated channel blocker gadolinium (1 mM) (5, 17), on the ischemia-induced ACh release.

Statistical Analysis

All data are presented as mean (SD) values. In *protocol 1*, we compared stimulation-induced ACh release among the five groups using one-way analysis of variance followed by the Student-Neuman-Keuls test (6). In *protocol 2*, we used an unpaired-*t* test (two-sided) to examine the effect of intravenous verapamil administration on stimulation-induced ACh release. In *protocol 3*, we compared ischemia-induced ACh release among the seven groups using one-way analysis of variance followed by the Dunnett' test against the control. For all analyses, differences were considered significant when $P < 0.05$.

RESULTS

In *protocol 1*, the ACh level during electrical vagal stimulation was 22.4 nM (SD 10.6). Local administration of verapamil did not affect stimulation-induced ACh release (Fig. 1). In contrast, local administration of ω-conotoxin GVIA or ω-conotoxin MVIIC suppressed stimulation-induced ACh release. The extent of suppression was greater in the latter. The ACh level was significantly lower in the simultaneous administration group (ω-conotoxin GVIA + ω-conotoxin MVIIC)

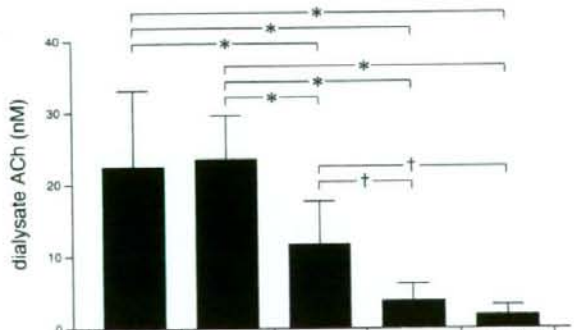

	vehicle	verapamil	ω-CTX GVIA	ω-CTX MVIIC	ω-CTX MVIIC + ω-CTX GVIA
vehicle		0.758	0.0054	0.0002	0.0002
verapamil	0.758		0.0068	0.0002	0.0001
GVIA	0.0054	0.0068		0.033	0.025
MVIIC	0.0002	0.0002	0.033		0.581
MVIIC+GVIA	0.0002	0.0001	0.025	0.581	

Fig. 1. Effects of local administration of verapamil, ω-conotoxin GVIA, ω-conotoxin MVIIC, or ω-conotoxin GVIA plus ω-conotoxin MVIIC on vagal nerve stimulation-induced myocardial interstitial ACh release. Both ω-conotoxin GVIA and ω-conotoxin MVIIC, but not verapamil, suppressed stimulation-induced ACh release. Data are mean (SD) values. *$P < 0.01$, †$P < 0.05$. The exact P values are presented.

than that in the ω-conotoxin GVIA group but was not different from the ω-conotoxin MVIIC group.

In *protocol 2*, the intravenous administration of verapamil did not significantly change stimulation-induced ACh release [21.7 nM (SD 12.8)] compared with the control group (P = 0.91).

In *protocol 3*, the ACh level in the ischemic region was 14.9 nM (SD 8.3) during 45–60 min of acute myocardial ischemia. Inhibition of voltage-dependent Ca^{2+} channels by local administration of verapamil, ω-conotoxin GVIA, or ω-conotoxin MVIIC did not affect ischemia-induced ACh release (Fig. 2). Inhibition of the reverse mode action of Na^+/Ca^{2+} exchange by local administration of KB-R7943 appeared to have augmented rather than suppressed ischemia-induced ACh release, though there was no statistically significant difference from the control. Blockade of the Ins(1,4,5)P_3 receptor by local administration of xestospongin C did not affect the ischemia-induced ACh release. In contrast, blockade of nonselective cation channels or cation-selective stretch-activated channels by local administration of gadolinium suppressed the ischemia-induced ACh release.

DISCUSSION

Ca^{2+} Channels Involved in Stimulation-Induced ACh Release

Although neurotransmitter release at mammalian sympathetic neuroeffector junctions predominantly depends on Ca^{2+} influx through N-type Ca^{2+} channels (23, 33, 34), the type(s) of Ca^{2+} channels involved in ACh release from cardiac parasympathetic neuroeffector junctions show diversity among reports (8, 28). One possible factor hampering investigations into parasympathetic postganglionic neurotransmitter release in response to vagal nerve stimulation in vivo is that the parasympathetic ganglia are usually situated in the vicinity of the effector organs, thereby making it difficult to separately assess ACh release from preganglionic and postganglionic nerves. In the previous study from our laboratory, intravenous administration, but not local administration of a ganglionic blocker, hexamethonium reduced vagal stimulation-induced ACh release assessed by cardiac microdialysis (1). The negligible effect of local hexamethonium administration on stimulation-induced ACh release suggests the lack of parasympathetic ganglia around the dialysis probe. In support of our speculation, a recent neuroanatomical finding indicates that three ganglia, away from the left anterior free wall targeted by the dialysis probe, provide the major source for left ventricular postganglionic innervation in cats: a cranioventricular ganglion, a left ventricular ganglion 2 (so designated), and an interventriculo-septal ganglion (11). Therefore, ACh, as measured by cardiac microdialysis, is considered to predominantly reflect ACh release from parasympathetic postganglionic nerves.

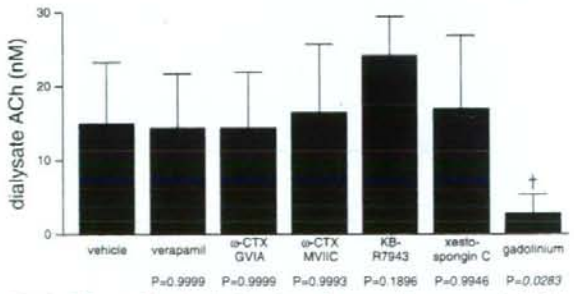

Fig. 2. Effects of local administration of verapamil, ω-conotoxin GVIA, ω-conotoxin MVIIC, KB-R7943, xestospongin C, or gadolinium on acute myocardial ischemia-induced myocardial interstitial ACh release in the ischemic region. Gadolinium alone suppressed the ischemia-induced ACh release. Data are mean (SD) values. †$P < 0.05$. The exact P values are presented.

Local (*protocol 1*) or intravenous (*protocol 2*) administration of verapamil did not affect stimulation-induced ACh release. In contrast, vagal stimulation-induced ACh release was reduced in both the ω-conotoxin GVIA and ω-conotoxin MVIIC groups but to a greater extent in the latter (Fig. 1). Therefore, both N- and P/Q-type, but probably not L-type, Ca^{2+} channels are involved in stimulation-induced ACh release from the cardiac parasympathetic postganglionic nerves in cats. The contribution of P/Q type Ca^{2+} channels to ACh release might be greater than that of N-type Ca^{2+} channels. Hong and Chang (8) reported that the negative inotropic response to field stimulation depends predominantly on the P/Q-type Ca^{2+} channels in isolated guinea pig atria, whereas Serone et al. (28) reported the predominance of N-type Ca^{2+} channels. In those studies, the field stimulation employed differed from ordinary activation of the postganglonic nerves by nerve discharge and, in addition, ACh release was not directly measured. The present study directly demonstrated the involvement of P/Q- and N-type Ca^{2+} channels in the stimulation-induced ACh release in the cardiac parasympathetic postganglionic nerves. These results support the concept that multiple subtypes of the voltage-gated Ca^{2+} channel mediate transmitter release from the same population of parasympathetic neurons (31).

Stimulation-induced ACh release was suppressed by ~50% in the ω-conotoxin GVIA group and by ~80% in the ω-conotoxin MVIIC group. The algebraic summation of the extent of suppression exceeded 100%. The phenomenon may be in part due to the nonlinear dose-response relationship between Ca^{2+} influx and transmitter release (32). The supra-additive phenomenon may be also due to the affinity of ω-conotoxin MVIIC to N-type Ca^{2+} channels (8, 26, 36). Combined local administration of ω-conotoxin GVIA and ω-conotoxin MVIIC almost completely suppressed stimulation-induced ACh release to a level similar to that achieved by the Na^+ channel inhibitor tetrodotoxin (15). Therefore, involvement of another untested type of Ca^{2+} channel(s) is unlikely in the stimulation-induced ACh release from the cardiac parasympathetic postganglionic nerves in cats.

Ca^{2+} Channels and Ischemia-Induced ACh Release

In a previous study, we showed that acute myocardial ischemia evokes myocardial interstitial ACh release in the ischemic region via a local mechanism independent of efferent vagal nerve activity (14). In that study, the inhibition of intracellular Ca^{2+} mobilization by local administration of 3,4,5-trimethoxybenzoic acid 8-(diethyl amino)-octyl ester (TMB-8) suppressed ischemia-induced ACh release, suggesting that an axoplasmic Ca^{2+} elevation is essential for the ischemia-induced ACh release. Because tissue K^+ concentration increases in the ischemic region (7, 18), high K^+-induced

depolarization could activate voltage-dependent Ca^{2+} channels even in the absence of efferent vagal nerve activity. However, ischemia-induced ACh release was not suppressed by local administration of verapamil, ω-conotoxin GVIA, or ω-conotoxin MVIIC (Fig. 2). Therefore, Ca^{2+} entry through the voltage-dependent Ca^{2+} channels is unlikely a mechanism for the ischemia-induced myocardial interstitial ACh release.

Acute myocardial ischemia causes energy depletion in the ischemic region, which impairs Na^+-K^+-ATPase activity. Ischemia also causes acidosis in the ischemic region, which promotes Na^+/H^+ exchange. As a result, ischemia causes intracellular Na^+ accumulation. The decrease in the Na^+ gradient across the plasma membrane may then cause the Na^+/Ca^{2+} exchanger to operate in the reverse mode, facilitating intracellular Ca^{2+} overload. KB-R7943 can inhibit the reverse mode of Na^+/Ca^{2+} exchange (9, 10) and its potential to protect against ischemia-reperfusion injury has been reported (21). In the present study, however, local administration of KB-R7943 failed to suppress and rather increased ACh release during ischemia as opposed to our expectation. It is plausible that the inhibition of reverse mode of Na^+/Ca^{2+} may have facilitated the accumulation of intracellular Na^+ and induced adverse effects that cancelled the possible beneficial effects derived from the inhibition of Ca^{2+} entry through the Na^+/Ca^{2+} exchanger itself. In addition, KB-R7943 could inhibit the forward mode of Na^+/Ca^{2+} exchange and reduce Ca^{2+} efflux (16), contributing to the intracellular Ca^{2+} accumulation and ACh release. In the present study, we observed the effects of KB-R7943 only during the ischemic period. However, accumulation of intracellular Na^+ through Na^+/H^+ exchange is enhanced on reperfusion due to the washout of extracellular H^+ (20). The inhibition of Na^+/Ca^{2+} exchange to suppress Ca^{2+} overload might become more important during the reperfusion phase. For instance, the percent segment shortening of the left ventricle was improved by KB-R7943 during reperfusion but not during ischemia (35).

As already mentioned, the ischemia-induced ACh release can be blocked by TMB-8 and thus the intracellular Ca^{2+} mobilization is required for the ischemia-induced ACh release (14). Besides the Ca^{2+} entries through voltage-dependent Ca^{2+} channels and via the reverse mode of Na^+/Ca^{2+} exchanger, Ca^{2+} may be mobilized from the endoplasmic reticulum via pathological pathways. As an example, the mitochondrial permeability transition pore triggered in pathological conditions is linked to cytochrome *c* release. Cytochrome *c* can bind to the endoplasmic reticulum $Ins(1,4,5)P_3$ receptor, rendering the channel insensitive to autoinhibition by high cytosolic Ca^{2+} concentration and resulting in enhanced endoplasmic reticulum Ca^{2+} release (4, 30). In the present study, however, blockade of $Ins(1,4,5)P_3$ receptor by xestospongin C failed to suppress the ischemia-induced ACh release. In contrast, local administration of gadolinium significantly suppressed the ischemia-induced ACh release. Therefore, nonselective cation channels or cation-selective stretch-activated channels contribute to the ischemia-induced ACh release. During myocardial ischemia, the ischemic region can be subjected to paradoxical systolic bulging. Such bulging likely opens stretch-activated channels and causes myocardial interstitial ACh release, possibly leading to cardioprotection by ACh against ischemic injury (2).

Limitations

First, the experiment was performed under anesthetic conditions, which may have influenced basal autonomic activity. However, because we sectioned the vagi at the neck, basal autonomic activity may have had only a minor effect on ACh release during the vagal stimulation and during acute myocardial ischemia. Second, we added eserine to the perfusate to inhibit immediate degradation of ACh (24), which may have increased the ACh level in the synaptic cleft and activated regulatory pathways such as autoinhibition of ACh release via muscarinic receptors (24). However, the myocardial interstitial ACh level measured under this condition could reflect changes induced by Na^+ channel inhibitor, choline uptake inhibitor, and vesicular ACh transport inhibitor as described in a previous study (15). Therefore, we think that the interpretation of the present results is reasonable. Third, tissue and species differences should be taken into account when extrapolating the present findings, because significant heterogeneity in the Ca^{2+} channels involved in the mammalian parasympathetic system may exist. Finally, we used verapamil to test the involvement of L-type Ca^{2+} channels in the ACh release. There are three major types of L-type Ca^{2+} channel antagonists with different binding domains (verapamil, nifedipine, and diltiazem) (19). Whether the effects on the ACh release are common among the three types of L-type Ca^{2+} channel antagonists remains unanswered.

In conclusion, the N- and P/Q-type Ca^{2+} channels (with the P/Q-type dominant), but probably not the L-type Ca^{2+} channels, are involved in vagal stimulation-induced ACh release from the cardiac parasympathetic postganglionic nerves in cats. In contrast, myocardial interstitial ACh release in the ischemic myocardium is resistant to the blockade of L-, N-, and P/Q-type Ca^{2+} channels. In addition, the ischemia-induced myocardial ACh release is resistant to the inhibition of Na^+/Ca^{2+} exchanger and the blockade of $Ins(1,4,5)P_3$ receptor but is suppressed by gadolinium, suggesting that nonselective cation channels or cation-selective stretch-activated channels are involved.

GRANTS

This study was supported by Health and Labour Sciences Research Grant for Research on Advanced Medical Technology from the Ministry of Health, Labour and Welfare of Japan, Health and Labour Sciences Research Grant for Research on Medical Devices for Analyzing, Supporting and Substituting the Function of Human Body from the Ministry of Health, Labour and Welfare of Japan, Health and Labour Sciences Research Grant H18-Iryo-Ippan-023 from the Ministry of Health, Labour and Welfare of Japan, Program for Promotion of Fundamental Studies in Health Science from the National Institute of Biomedical Innovation, a Grant provided by the Ichiro Kanehara Foundation, Ground-based Research Announcement for Space Utilization promoted by Japan Space Forum, and Industrial Technology Research Grant Program in 03A47075 from New Energy and Industrial Technology Development Organization of Japan.

REFERENCES

1. **Akiyama T, Yamazaki T, and Ninomiya I.** In vivo detection of endogenous acetylcholine release in cat ventricles. *Am J Physiol Heart Circ Physiol* 266: H854–H860, 1994.
2. **Ando M, Katare RG, Kakinuma Y, Zhang D, Yamasaki F, Muramoto K, and Sato T.** Efferent vagal nerve stimulation protects heart against ischemia-induced arrhythmias by preserving connexin43 protein. *Circulation* 112: 164–170, 2005.

3. **Bibevski S and Dunlap ME.** Prevention of diminished parasympathetic control of the heart in experimental heart failure. *Am J Physiol Heart Circ Physiol* 287: H1780–H1785, 2004.
4. **Brookes PS, Yoon Y, Robotham JL, Anders MW, and Sheu SS.** Calcium, ATP, and ROS: a mitochondrial love-hate triangle. *Am J Physiol Cell Physiol* 287: C817–C833, 2004.
5. **Caldwell RA, Clemo HF, and Baumgarten CM.** Using gadolinium to identify stretch-activated channels: technical considerations. *Am J Physiol Cell Physiol* 275: C619–C621, 1998.
6. **Glantz SA.** *Primer of Biostatistics* (5th ed) New York: McGraw-Hill, 2002.
7. **Hirche HJ, Franz CHR, Bös L, Bissig R, Lang R, and Schramm M.** Myocardial extracellular K^+ and H^+ increase and noradrenaline release as possible cause of early arrhythmias following acute coronary artery occlusion in pigs. *J Mol Cell Cardiol* 12: 579–593, 1979.
8. **Hong SJ and Chang CC.** Calcium channel subtypes for the sympathetic and parasympathetic nerves of guinea-pig atria. *Br J Pharmacol* 116: 1577–1582, 1995.
9. **Iwamoto T, Kita S, Uehara A, Inoue Y, Taniguchi Y, Imanaga I, and Shigekawa M.** Structural domains influencing sensitivity to isothiourea derivative inhibitor KB-R7943 in cardiac Na^+/Ca^{2+} exchanger. *Mol Pharmacol* 59: 524–531, 2001.
10. **Iwamoto T, Watano T, and Shigekawa M.** A novel isothiourea derivative selectively inhibits the reverse mode of Na^+/Ca^{2+} exchange in cells expressing NCX1. *J Biol Chem* 271: 22391–22397, 1996.
11. **Johnson TA, Gray AL, Lauenstein JM, Newton SS, and Massari VJ.** Parasympathetic control of the heart. I. An interventriculo-septal ganglion is the major source of the vagal intracardiac innervation of the ventricles. *J Appl Physiol* 96: 2265–2272, 2004.
12. **Kawada T, Yamazaki T, Akiyama T, Inagaki M, Shishido T, Zheng C, Yanagiya Y, Sugimachi M, and Sunagawa K.** Vagosympathetic interactions in ischemia-induced myocardial norepinephrine and acetylcholine release. *Am J Physiol Heart Circ Physiol* 280: H216–H221, 2001.
13. **Kawada T, Yamazaki T, Akiyama T, Li M, Ariumi H, Mori H, Sunagawa K, and Sugimachi M.** Vagal stimulation suppresses ischemia-induced myocardial interstitial norepinephrine release. *Life Sci* 78: 882–887, 2006.
14. **Kawada T, Yamazaki T, Akiyama T, Sato T, Shishido T, Inagaki M, Takaki H, Sugimachi M, and Sunagawa K.** Differential acetylcholine release mechanisms in the ischemic and non-ischemic myocardium. *J Mol Cell Cardiol* 32: 405–414, 2000.
15. **Kawada T, Yamazaki T, Akiyama T, Shishido T, Inagaki M, Uemura K, Miyamoto T, Sugimachi M, Takaki H, and Sunagawa K.** In vivo assessment of acetylcholine-releasing function at cardiac vagal nerve terminals. *Am J Physiol Heart Circ Physiol* 281: H139–H145, 2001.
16. **Kimura J, Watano T, Kawahara M, Sakai E, and Yatabe J.** Direction-independent block of bi-directional Na^+/Ca^{2+} exchange current by KB-R7943 in guinea-ping cardiac myocytes. *Br J Pharmacol* 128: 969–974, 1999.
17. **Kimura S, Mieno H, Tamaki K, Inoue M, and Chayama K.** Nonselective cation channel as a Ca^{2+} influx pathway in pepsinogen-secreting cells of bullfrog esophagus. *Am J Physiol Gastrointest Liver Physiol* 281: G333–G341, 2001.
18. **Kléber AG.** Extracellular potassium accumulation in acute myocardial ischemia. *J Mol Cell Cardiol* 16: 389–394, 1984.
19. **Kurokawa J, Adachi-Akahane S, and Nagao T.** 1–5-Benzothiazepine binding domain is located on the extracellular side of the cardiac L-type Ca^{2+} channel. *Mol Pharmacol* 51: 262–268, 1997.
20. **Lazdunski M, Frelin C, and Vigne P.** The sodium/hydrogen exchange system in cardiac cells: its biochemical and pharmacological properties and its role in regulating internal concentrations of sodium and internal pH. *J Mol Cell Cardiol* 17: 1029–1042, 1985.
21. **Lee C, Dhalla NS, and Hryshko LV.** Therapeutic potential of novel Na^+-Ca^{2+} exchange inhibitors in attenuating ischemia-reperfusion injury. *Can J Cardiol* 21: 509–516, 2005.
22. **Li M, Zheng C, Sato T, Kawada T, Sugimachi M, and Sunagawa K.** Vagal nerve stimulation markedly improves long-term survival after chronic heart failure in rats. *Circulation* 109: 120–124, 2004.
23. **Molderings GJ, Likungu J, and Göthert M.** N-type calcium channels control sympathetic neurotransmission in human heart atrium. *Circulation* 101: 403–407, 2000.
24. **Nicholls DG.** *Proteins, Transmitters and Synapses*. Oxford: Blackwell Science, 1994.
25. **Oka T, Sato K, Hori M, Ozaki H, and Karaki H.** Xestospongin C, a novel blocker of IP_3 receptor, attenuates the increase in cytosolic calcium level and degranulation that is induced by antigen in RBL-2H3 mast cells. *Br J Pharmacol* 135: 1959–1966, 2002.
26. **Randall A and Tsien RW.** Pharmacological dissection of multiple types of Ca^{2+} channel currents in rat cerebellar granule neurons. *J Neurosci* 15: 2995–3012, 1995.
27. **Schauerte P, Scherlag BJ, Scherlag MA, Goli S, Jackman WM, and Lazzara R.** Ventricular rate control during atrial fibrillation by cardiac parasympathetic nerve stimulation: a transvenous approach. *J Am Coll Cardiol* 34: 2043–2050, 1999.
28. **Serone AP and Angus JA.** Role of N-type calcium channels in autonomic neurotransmission in guinea-pig isolated left atria. *Br J Pharmacol* 127: 927–934, 1999.
29. **Smith AB, Motin L, Lavidis NA, and Adams DJ.** Calcium channels controlling acetylcholine release from preganglionic nerve terminals in rat autonomic ganglia. *Neuroscience* 95: 1121–1127, 2000.
30. **Verkhratsky A and Toescu EC.** Endoplasmic reticulum Ca^{2+} homeostasis and neuronal death. *J Cell Mol Med* 4: 351–361, 2003.
31. **Waterman SA.** Multiple subtypes of voltage-gated calcium channel mediate transmitter release from parasympathetic neurons in the mouse bladder. *J Neurosci* 16: 4155–4161, 1996.
32. **Wheeler DB, Randall A, and Tsien RW.** Changes in action potential duration after reliance of excitatory synaptic transmission on multiple types of Ca^{2+} channels in rat hippocampus. *J Neurosci* 16: 2226–2237, 1996.
33. **Yahagi N, Akiyama T, and Yamazaki T.** Effects of ω-conotoxin GVIA on cardiac sympathetic nerve function. *J Auton Nerv Syst* 68: 43–48, 1998.
34. **Yamazaki T, Akiyama T, Kitagawa H, Takauchi Y, Kawada T, and Sunagawa K.** A new, concise dialysis approach to assessment of cardiac sympathetic nerve terminal abnormalities. *Am J Physiol Heart Circ Physiol* 272: H1182–H1187, 1997.
35. **Yoshitomi O, Akiyama D, Hara T, Cho S, Tomiyasu S, and Sumikawa K.** Cardioprotective effects of KB-R7943, a novel inhibitor of Na^+/Ca^{2+} exchanger, on stunned myocardium in anesthetized dogs. *J Anesth* 19: 124–130, 2005.
36. **Zhang JF, Randall AD, Ellinor PT, Horne WA, Sather WA, Tanabe T, Schwarz TL, and Tsien RW.** Distinctive pharmacology and kinetics of cloned neuronal Ca^{2+} channels and their possible counterparts in mammalian CNS neurons. *Neuropharmacology* 32: 1075–1088, 1993.

J Appl Physiol 102: 622–627, 2007.
First published November 2, 2006; doi:10.1152/japplphysiol.00622.2006.

Hypothermia reduces ischemia- and stimulation-induced myocardial interstitial norepinephrine and acetylcholine releases

Toru Kawada,[1] Hirotoshi Kitagawa,[2] Toji Yamazaki,[2] Tsuyoshi Akiyama,[2] Atsunori Kamiya,[1] Kazunori Uemura,[1] Hidezo Mori,[2] and Masaru Sugimachi[1]

[1]*Department of Cardiovascular Dynamics, Advanced Medical Engineering Center, and*
[2]*Department of Cardiac Physiology, National Cardiovascular Center Research Institute, Osaka, Japan*

Submitted 4 June 2006; accepted in final form 1 November 2006

Kawada T, Kitagawa H, Yamazaki T, Akiyama T, Kamiya A, Uemura K, Mori H, Sugimachi M. Hypothermia reduces ischemia- and stimulation-induced myocardial interstitial norepinephrine and acetylcholine releases. *J Appl Physiol* 102: 622–627, 2007. First published November 2, 2006; doi:10.1152/japplphysiol.00622.2006.—Although hypothermia is one of the most powerful modulators that can reduce ischemic injury, the effects of hypothermia on the function of the cardiac autonomic nerves in vivo are not well understood. We examined the effects of hypothermia on the myocardial interstitial norepinephrine (NE) and ACh releases in response to acute myocardial ischemia and to efferent sympathetic or vagal nerve stimulation in anesthetized cats. We induced acute myocardial ischemia by coronary artery occlusion. Compared with normothermia ($n = 8$), hypothermia at 33°C ($n = 6$) suppressed the ischemia-induced NE release [63 nM (SD 39) vs. 18 nM (SD 25), $P < 0.01$] and ACh release [11.6 nM (SD 7.6) vs. 2.4 nM (SD 1.3), $P < 0.01$] in the ischemic region. Under hypothermia, the coronary occlusion increased the ACh level from 0.67 nM (SD 0.44) to 6.0 nM (SD 6.0) ($P < 0.05$) and decreased the NE level from 0.63 nM (SD 0.19) to 0.40 nM (SD 0.25) ($P < 0.05$) in the nonischemic region. Hypothermia attenuated the nerve stimulation-induced NE release from 1.05 nM (SD 0.85) to 0.73 nM (SD 0.73) ($P < 0.05$, $n = 6$) and ACh release from 10.2 nM (SD 5.1) to 7.1 nM (SD 3.4) ($P < 0.05$, $n = 5$). In conclusion, hypothermia attenuated the ischemia-induced NE and ACh releases in the ischemic region. Moreover, hypothermia also attenuated the nerve stimulation-induced NE and ACh releases. The Bezold-Jarisch reflex evoked by the left anterior descending coronary artery occlusion, however, did not appear to be affected under hypothermia.

vagal nerve; sympathetic nerve; cardiac microdialysis; cats

HYPOTHERMIA IS ONE OF THE most powerful modulators that can reduce ischemic injury in the central nervous system, heart, and other organs. The general consensus is that hypothermia induces a hypometabolic state in tissues and balances energy supply and demand (25). With respect to the myocardial ischemia, the size of a myocardial infarction correlates with temperature (6), and mild hypothermia can protect the myocardium against acute ischemic injury (9). The effects of hypothermia on the function of the cardiac autonomic nerves in terms of neurotransmitter releases, however, are not fully understood. Because autonomic neurotransmitters such as norepinephrine (NE) and ACh directly impinge on the myocardium, they would be implicated in the cardioprotection by hypothermia.

In previous studies from our laboratory, Kitagawa et al. (16) demonstrated that hypothermia attenuated the nonexocytotic NE release induced pharmacologically by ouabain, tyramine, or cyanide. Kitagawa et al. (15) also demonstrated that hypothermia attenuated the exocytotic NE release in response to vena cava occlusion or to local administration of high K^+. The effects of hypothermia on the ischemia-induced myocardial interstitial NE release, however, were not examined in those studies. In addition, the effects of hypothermia on the ischemia-induced myocardial interstitial ACh release have never been examined. Because both sympathetic and parasympathetic nerves control the heart, simultaneous monitoring of the myocardial interstitial releases of NE and ACh (14, 31) would help integrative understanding of the autonomic nerve terminal function under hypothermia in conjunction with acute myocardial ischemia.

In the present study, the effects of hypothermia on the ischemia-induced and nerve stimulation-induced myocardial interstitial neurotransmitter releases were examined. We implanted a dialysis probe into the left ventricular free wall of anesthetized cats and measured dialysate NE and ACh levels as indexes of neurotransmitter outputs from the cardiac sympathetic and vagal nerve terminals, respectively. Based on our laboratory's previous results (15, 16), we hypothesized that hypothermia would attenuate the neurotransmitter releases in response to acute myocardial ischemia and to electrical nerve stimulation.

MATERIALS AND METHODS

Surgical Preparation and Protocols

Animals were cared for in accordance with the *Guiding Principles for the Care and Use of Animals in the Field of Physiological Sciences*, approved by the Physiological Society of Japan. All protocols were reviewed and approved by the Animal Subjects Committee of National Cardiovascular Center. Adult cats were anesthetized via an intraperitoneal injection of pentobarbital sodium (30–35 mg/kg) and ventilated mechanically through an endotracheal tube with oxygen-enriched room air. The level of anesthesia was maintained with a continuous intravenous infusion of pentobarbital sodium (1–2 $mg \cdot kg^{-1} \cdot h^{-1}$) through a catheter inserted from the right femoral vein. Mean arterial pressure (MAP) was measured using a pressure transducer connected to a catheter inserted from the right femoral artery. Heart rate (HR) was determined from an electrocardiogram.

Protocol 1: acute myocardial ischemia. We examined the effects of hypothermia on the ischemia-induced myocardial interstitial releases of NE and ACh. The heart was exposed by partially removing the left fifth and/or sixth rib. A dialysis probe was implanted transversely into

Address for reprint requests and other correspondence: T. Kawada, Dept. of Cardiovascular Dynamics, Advanced Medical Engineering Center, National Cardiovascular Center Research Institute, 5-7-1 Fujishirodai, Suita, Osaka 565-8565, Japan (e-mail: torukawa@res.ncvc.go.jp).

The costs of publication of this article were defrayed in part by the payment of page charges. The article must therefore be hereby marked "*advertisement*" in accordance with 18 U.S.C. Section 1734 solely to indicate this fact.

the anterolateral free wall of the left ventricle perfused by the left anterior descending coronary artery (LAD) to monitor myocardial interstitial NE and ACh levels in the ischemic region during occlusion of the LAD (13). Another dialysis probe was implanted transversely into the posterior free wall of the left ventricle perfused by the left circumflex coronary artery to monitor myocardial interstitial NE and ACh levels in a nonischemic region. Heparin sodium (100 U/kg) was administered intravenously to prevent blood coagulation. Animals were divided into a normothermic group ($n = 8$) and a hypothermic group ($n = 6$). In the hypothermic group, surface cooling with ice bags was performed until the esophageal temperature decreased to 33°C (15, 16). A stable hypothermic condition was obtained within ~2 h. In each group, we occluded the LAD for 60 min and examined changes in the myocardial interstitial NE and ACh levels in the ischemic region (i.e., the LAD region) and nonischemic region (i.e., the left circumflex coronary artery region). Fifteen-minute dialysate samples were obtained during the preocclusion baseline condition and during the periods of 0–15, 15–30, 30–45, and 45–60 min of the LAD occlusion.

Protocol 2: sympathetic stimulation. We examined the effects of hypothermia on the sympathetic nerve stimulation-induced myocardial interstitial NE release ($n = 6$). A dialysis probe was implanted transversely into the anterolateral free wall of the left ventricle. The bilateral cardiac sympathetic nerves originating from the stellate ganglia were exposed through a second intercostal space and sectioned. The cardiac end of each sectioned nerve was placed on a bipolar platinum electrode for sympathetic stimulation (5 Hz, 10 V, 1-ms pulse duration). The electrodes and nerves were covered with mineral oil to provide insulation and prevent desiccation. A 4-min dialysate sample was obtained during the sympathetic stimulation under the normothermic condition. Thereafter, hypothermia was introduced using the same cooling procedure as in *protocol 1*, and a second 4-min dialysate sample was obtained during the sympathetic stimulation.

Protocol 3: vagal stimulation. We examined the effects of hypothermia on the vagal nerve stimulation-induced ACh release ($n = 5$). A dialysis probe was implanted transversely into the anterolateral free wall of the left ventricle. The bilateral vagi were exposed through a midline cervical incision and sectioned at the neck. The cardiac end of each sectioned nerve was placed on a bipolar platinum electrode for vagal stimulation (20 Hz, 10 V, 1-ms pulse duration). To prevent severe bradycardia and cardiac arrest, which can be induced by the vagal stimulation, the heart was paced at 200 beats/min using pacing wires attached to the apex of the heart during the stimulation period. A 4-min dialysate sample was obtained during the vagal stimulation under the normothermic condition. Thereafter, hypothermia was introduced using the same cooling procedure as in *protocol 1*, and a second 4-min dialysate sample was obtained during the vagal stimulation.

Because of the relatively intense stimulation of the sympathetic or vagal nerve, the stimulation period in *protocols 2* and *3* was limited to 4 min to minimize gradual waning of the stimulation effects. At the end of the experiment, the animals were killed by increasing the depth of anesthesia with an overdose of pentobarbital sodium. We then confirmed that the dialysis probes had been threaded in the middle layer of the left ventricular myocardium.

Dialysis Technique

The dialysate NE and ACh concentrations were measured as indexes of myocardial interstitial NE and ACh levels, respectively. The materials and properties of the dialysis probe have been described previously (2, 3). Briefly, we designed a transverse dialysis probe. A dialysis fiber (13-mm length, 310-μm outer diameter, 200-μm inner diameter; PAN-1200, 50,000 molecular weight cutoff; Asahi Chemical) was connected at both ends to polyethylene tubes (25-cm length, 500-μm outer diameter, 200-μm inner diameter). The dialysis probe was perfused with Ringer solution containing a cholinesterase inhibitor eserine (10^{-4} M) at a rate of 2 μl/min. We started dialysate sampling from 2 h after the implantation of the dialysis probe(s), when the dialysate NE and ACh concentrations had reached steady states. The actual dialysate sampling was delayed by 5 min from the collection period to account for the dead space volume between the semipermeable membrane and the sample tube. Each sample was collected in a microtube containing 3 μl of HCl to prevent amine oxidation. The dialysate ACh concentration was measured directly by HPLC with electrochemical detection (Eicom). The in vitro recovery rate of ACh was ~70%. With the use of a criterion of signal-to-noise ratio of higher than three, the detection limit for ACh was 3 pg per injection. The dialysate NE concentration was measured by another HPLC-electrochemical detection system after the removal of interfering compounds by an alumina procedure. The in vitro recovery rate of NE was ~55%. With the use of a criterion of signal-to-noise ratio of higher than three, the detection limit for NE was 200 fg per injection.

Statistical Analysis

All data are presented as means and SD values. For *protocol 1*, we performed two-way repeated-measures ANOVA using hypothermia as one factor and the dialysate sampling periods (the effects of ischemia) as the other factor. For *protocols 2* and *3*, we compared stimulation-induced releases of NE and ACh before and during hypothermia using a paired *t*-test. For all of the statistics, the difference was considered significant when $P < 0.05$.

RESULTS

Figure 1*A* illustrates changes in myocardial interstitial NE levels in the ischemic region during LAD occlusion obtained from *protocol 1*. The *inset* shows the magnified ordinate for the

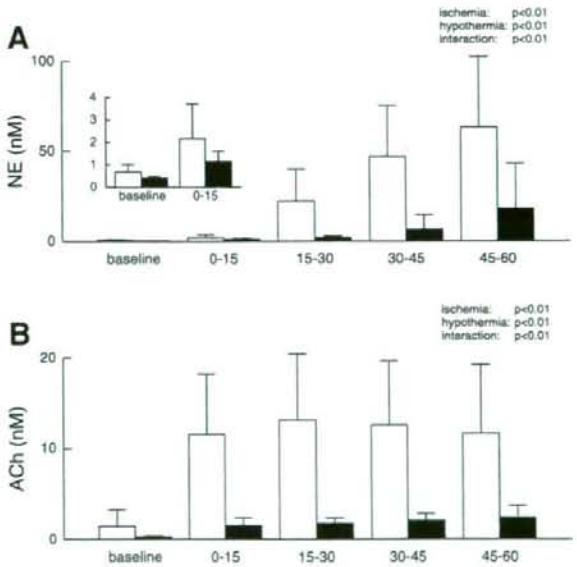

Fig. 1. *A*: ischemia-induced myocardial interstitial norepinephrine (NE) release in the ischemic region. Acute myocardial ischemia caused a progressive increase in the level of myocardial interstitial NE. Hypothermia attenuated the ischemia-induced NE release. *Inset*: magnified ordinate for the baseline and the 0- to 15-min period of ischemia. *B*: ischemia-induced myocardial interstitial ACh release in the ischemic region. Acute myocardial ischemia increased the myocardial interstitial ACh levels. Hypothermia attenuated the ischemia-induced ACh release. Open bars: normothermia; solid bars: hypothermia.

baseline and the 0- to 15-min period of ischemia. In the normothermic group (open bars), the LAD occlusion caused an ~94-fold increase in the NE level during the 45- to 60-min interval. In the hypothermic group (solid bars), the LAD occlusion caused an ~45-fold increase in the NE level during the 45- to 60-min interval. Compared with normothermia, hypothermia suppressed the baseline NE level to ~59% and the NE level during the 45- to 60-min period to ~29%. Statistical analysis indicated that the effects of both hypothermia and ischemia on the NE release were significant, and the interaction between hypothermia and ischemia was also significant.

Figure 1*B* illustrates changes in myocardial interstitial ACh levels in the ischemic region during the LAD occlusion. In both the normothermic (open bars) and hypothermic (solid bars) groups, the LAD occlusion caused an approximately eightfold increase in the ACh level during the 45- to 60-min interval. Compared with normothermia, however, hypothermia suppressed both the baseline ACh level and the ACh level during the 45- to 60-min period of ischemia to ~20%. Statistical analysis indicated that the effects of both hypothermia and ischemia on the ACh release were significant, and the interaction between hypothermia and ischemia was also significant.

Figure 2*A* illustrates changes in myocardial interstitial NE levels in the nonischemic region during the LAD occlusion. Note that scale of the ordinate is only one-hundredth of that in Fig. 1*A*. The LAD occlusion decreased the NE level in the normothermic group (open bars); the NE level during the 45- to 60-min interval was ~59% of the baseline level. The LAD occlusion also decreased the NE level in the hypothermic group (solid bars); the NE level during the 45- to 60-min interval was ~64% of the baseline level. Although the LAD occlusion resulted in a decrease in the NE level under both conditions, the NE level under hypothermia was nearly twice that measured under normothermia. The statistical analysis indicated that the effects of both hypothermia and ischemia on the NE release were significant, whereas the interaction between hypothermia and ischemia was not significant.

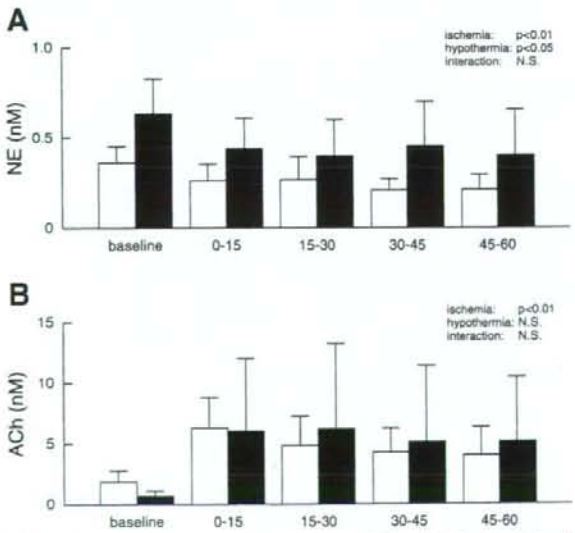

Fig. 2. *A*: changes in the myocardial interstitial NE levels in the nonischemic region. Acute myocardial ischemia decreased the level of myocardial interstitial NE from the baseline level. Hypothermia increased the myocardial interstitial NE levels in the nonischemic region. *B*: changes in the myocardial interstitial ACh levels in the nonischemic region. Acute myocardial ischemia increased the myocardial interstitial ACh level. Hypothermia did not attenuate the increasing response of ACh to the left anterior descending coronary artery occlusion. Open bars: normothermia; solid bars: hypothermia. NS, not significant.

Table 1. *Mean arterial pressure during acute myocardial ischemia obtained in protocol 1*

	Baseline	5 min	15 min	30 min	45 min	60 min
Normothermia	108 (23)	102 (28)	101 (24)	101 (20)	102 (21)	102 (21)
Hypothermia	108 (11)	80 (17)	87 (10)	85 (10)	86 (10)	91 (11)

Values are means (SD) (in mmHg) obtained during preocclusion baseline period and 5-, 15-, 30-, 45-, and 60-min periods of coronary artery occlusion. Ischemia: $P < 0.01$; hypothermia: not significant; interaction: $P < 0.01$.

Figure 2*B* illustrates changes in myocardial interstitial ACh levels in the nonischemic region during the LAD occlusion. The LAD occlusion caused an ~3.4-fold increase in the ACh level during the 0- to 15-min interval in the normothermic group (open bars). The LAD occlusion caused an approximately ninefold increase in the ACh level during the 0- to 15-min interval in the hypothermic group (solid bars). These effects of ischemia on the ACh release were statistically significant. Although hypothermia seemed to attenuate the baseline ACh level, the overall effects of hypothermia on the ACh level were insignificant.

Tables 1 and 2 summarize the MAP and HR data, respectively, obtained in *protocol 1*. Acute myocardial ischemia significantly reduced MAP ($P < 0.01$) and HR ($P < 0.01$). Hypothermia did not affect MAP but did decrease HR ($P < 0.01$). The interaction between ischemia and hypothermia was significant for MAP but not for HR by the two-way repeated-measures ANOVA.

For *protocol 2*, hypothermia significantly attenuated the sympathetic stimulation-induced NE release to ~70% of the level observed during normothermia (Fig. 3*A*). Under normothermia, the sympathetic stimulation increased MAP from 114 mmHg (SD 27) to 134 mmHg (SD 33) ($P < 0.01$) and HR from 147 beats/min (SD 9) to 207 beats/min (SD 5) ($P < 0.01$). Under hypothermia, the sympathetic stimulation increased MAP from 117 mmHg (SD 11) to 136 mmHg (SD 22) ($P < 0.05$) and HR from 125 beats/min (SD 16) to 164 beats/min (SD 10) ($P < 0.01$).

For *protocol 3*, hypothermia significantly attenuated the vagal stimulation-induced ACh release to ~70% of the level observed during normothermia (Fig. 3*B*). Hypothermia did not change MAP [117 mmHg (SD 18) vs. 118 mmHg (SD 27)] but

Table 2. *Heart rate during acute myocardial ischemia obtained in protocol 1*

	Baseline	5 min	15 min	30 min	45 min	60 min
Normothermia	183 (26)	160 (18)	163 (16)	163 (18)	166 (20)	165 (21)
Hypothermia	146 (25)	116 (19)	113 (19)	126 (39)	112 (20)	97 (31)

Values are means (SD) (in beats/min) obtained during preocclusion baseline period and 5-, 15-, 30-, 45-, and 60-min periods of coronary artery occlusion. Ischemia: $P < 0.01$; hypothermia: $P < 0.01$; interaction: not significant.

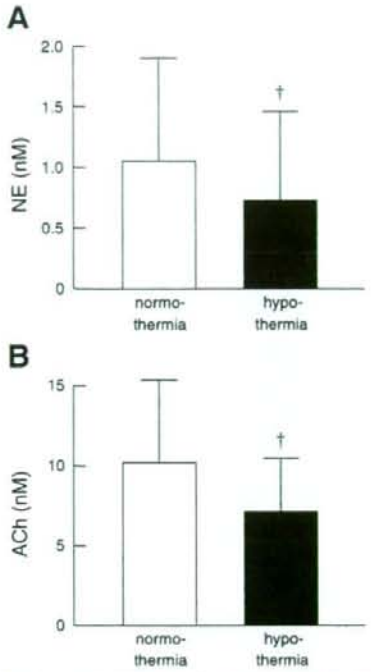

Fig. 3. *A*: efferent sympathetic nerve stimulation-induced release of myocardial interstitial NE before and during hypothermia. †Hypothermia significantly attenuated the stimulation-induced NE release. *B*: efferent vagal nerve stimulation-induced release of myocardial interstitial ACh before and during hypothermia. †Hypothermia significantly attenuated the stimulation-induced ACh release.

did decrease HR from 202 beats/min (SD 24) to 179 beats/min (SD 15) ($P < 0.05$) during the prestimulation, unpaced condition. MAP during the stimulation was 105 mmHg (SD 19) under normothermia and 93 mmHg (SD 33) under hypothermia.

DISCUSSION

A cardiac microdialysis is a powerful tool to estimate neurotransmitter levels in the myocardial interstitium in vivo (2, 3, 14, 19, 20, 31). The present study demonstrated that hypothermia significantly attenuated the myocardial interstitial releases of NE and ACh in the ischemic region during the LAD occlusion. In contrast, the increasing response in the ACh level from its baseline level and the decreasing response in the NE level from its baseline level observed in the nonischemic region were maintained under hypothermia. To our knowledge, this is the first report showing the effects of hypothermia on the myocardial interstitial releases of NE and ACh during acute myocardial ischemia in vivo. In addition, the present study showed that hypothermia significantly attenuated nerve stimulation-induced myocardial interstitial NE and ACh releases in vivo.

Effects of Hypothermia on Ischemia-induced NE and ACh Releases in the Ischemic Region

Acute myocardial ischemia causes energy depletion, which leads to myocardial interstitial NE release in the ischemic region (Fig. 1*A*). The NE release can be classified as exocytotic or nonexocytotic (18, 24). Exocytotic release indicates NE release from synaptic vesicles, which normally occurs in response to nerve discharge and subsequent Ca^{2+} influx through voltage-dependent Ca^{2+} channels. On the other hand, nonexocytotic release indicates NE release from the axoplasm, such as that mediated by a reverse transport through the NE transporter. A neuronal uptake blocker, desipramine, can suppress the ischemia-induced NE release (19, 24). Whereas exocytotic release contributes to the ischemia-induced NE release in the initial phase of ischemia (within ~20 min), carrier-mediated nonexocytotic release becomes predominant as the ischemic period is prolonged (1). Hypothermia significantly attenuated the ischemia-induced NE release (Fig. 1*A*). The NE level during the 45- to 60-min period of ischemia under hypothermia was ~20% of that obtained under normothermia. The NE uptake transporter is driven by the Na^+ gradient across the cell membrane (23). The loss of the Na^+ gradient due to ischemia causes NE to be transported out of the cell by reversing the action of the NE transporter. Hypothermia inhibits the action of the NE transporter and also suppresses the intracellular Na^+ accumulation (8), thereby reducing nonexocytotic NE release during ischemia. The present results are in line with an in vitro study that showed hypothermia suppressed nonexocytotic NE release induced by deprivation of oxygen and glucose (30). The present results are also consistent with a previous study from our laboratory that showed hypothermia attenuated the nonexocytotic NE release induced by ouabain, tyramine, or cyanide (16).

Acute myocardial ischemia increases myocardial interstitial ACh level in the ischemic region, as reported previously (Fig. 1*B*) (13). The level of ischemia-induced ACh release during 0- to 15-, 15- to 30-, 30- to 45-, or 45- to 60-min period of ischemia is comparable to that evoked by 4-min electrical stimulation of the bilateral vagi (Fig. 3*B*). Compared with the normothermic condition, hypothermia significantly attenuated the ischemia-induced myocardial interstitial release of ACh in the ischemic region. Our laboratory's previous study indicated that intracellular Ca^{2+} mobilization is essential for the ischemia-induced release of ACh (13). Hypothermia may have prevented the Ca^{2+} overload, thereby reducing the ischemia-induced ACh release. Alternatively, hypothermia may reduce the extent of the ischemic injury, which in turn suppressed the ischemia-induced ACh release. Because ACh has protective effects on the cardiomyocytes against ischemia (11), the suppression of ischemia-induced ACh release during hypothermia itself may be unfavorable for cardioprotection.

There is considerable controversy regarding the cardioprotective effects of β-adrenergic blockade during severe ischemia, with studies demonstrating a reduction of infarct size (10, 17) or no effects (7, 27). The β-adrenergic blockade seems effective to protect the heart only when the heart is reperfused within a certain period after the coronary occlusion. The β-adrenergic blockade would reduce the myocardial oxygen consumption through the reduction of HR and ventricular contractility and delay the progression of ischemic injury. Hence the infarct size might be reduced when the heart is reperfused before the ischemic damage becomes irreversible. The ischemia-induced NE release reached nearly 100 times the baseline NE level under normothermia (Fig. 1*A*), which by far exceeded the NE level attained by electrical stimulation of the

bilateral stellate ganglia (Fig. 3*A*). Because high NE levels have cardiotoxic effects (22), ischemia-induced NE release might aggravate the ischemic injury. However, catecholamine depletion by a reserpine treatment fails to reduce the infarct size (26, 29), throwing a doubt on the involvement of catecholamine toxicity in the progression of myocardial damage during ischemia. It is, therefore, most likely that the hypothermia-induced reductions in NE and ACh are the result of reduced myocardial damage or a direct effect on nerve endings.

Van den Doel et al. (28) showed that hypothermia does not abolish necrosis, but rather delays necrosis during sustained ischemia, so that hypothermia protected against infarction produced by a 30-min occlusion but not against infarction produced by a 60-min occlusion in the rat heart. At the same time, they mentioned that hypothermia was able to reduce the infarct size after a 60-min coronary occlusion in the dog, possibly because of the significant collateral flow in the canine hearts. Because the feline hearts are similar to the canine hearts in that they have considerable collateral flow compared with the rat hearts (21), hypothermia should have protected the feline heart against the 60-min coronary occlusion in the present study.

Effects of Hypothermia on the NE and ACh Releases in the Nonischemic Region and on the Electrical Stimulation-induced NE and ACh Releases

The NE and ACh levels in the nonischemic region may reflect the sympathetic and parasympathetic drives to this region. As an example, myocardial interstitial ACh levels increase during activations of the arterial baroreflex and the Bezold-Jarisch reflex (14). In the present study, acute myocardial ischemia decreased the NE level from its baseline level, whereas it increased the ACh level from its baseline level (Fig. 2). Ischemia also decreased MAP and HR (Tables 1 and 2), suggesting that the Bezold-Jarisch reflex was induced by the LAD occlusion under both normothermia and hypothermia. Taking into account the fact that electrical stimulation-induced ACh release was attenuated to ~70% (Fig. 3), similar ACh levels during ischemia imply the enhancement of the parasympathetic outflow via the Bezold-Jarisch reflex under hypothermia. These results are in line with the study by Zheng et al. (32), where pulmonary chemoreflex-induced bradycardia was maintained under hypothermia. Hypothermia increased the NE level in the nonischemic region, suggesting that sympathetic drive to this region also increased. Hypothermic stress is known to cause sympathetic activation, accompanying increases in MAP, HR, plasma NE, and epinephrine levels (4). In the present study, because the effect of hypothermia on MAP was insignificant (Table 1) and HR decreased under hypothermia (Table 2), the sympathetic activation observed in the nonischemic region might have been regional and not systemic.

Hypothermia attenuated the releases of NE and ACh in response to respective nerve stimulation to ~70% of that observed under normothermia (Fig. 3). The suppression of the exocytotic NE release by hypothermia is consistent with a previous study from our laboratory, where hypothermia attenuated the myocardial interstitial NE release in response to vena cava occlusion or to a local high K^+ administration (15). The suppression of NE release by hypothermia is consistent with an in vitro study by Kao and Westhead (12) in which catecholamine secretion from adrenal chromaffin cells induced by elevated K^+ levels increased as the temperature increased from 4 to 37°C. On the other hand, because hypothermia inhibits the neuronal NE uptake, the NE concentration at the synaptic cleft is expected to be increased if the level of NE release remains unchanged. Actually, Vizi (30) demonstrated that hypothermia increased NE release in response to field stimulation in vitro. In the present study, however, the suppression of NE release might have canceled the potential accumulation of NE due to NE uptake inhibition. The present study also demonstrated that the ACh release was suppressed by hypothermia. In the rat striatum, hypothermia decreases the extracellular ACh concentration and increases the choline concentration (5). Hypothermia may inhibit a choline uptake transporter in the same manner as it inhibits a NE uptake transporter. The inhibition of the choline transporter by hypothermia may have hampered the replenishment of the available pool of ACh and thereby contributed to the suppression of the stimulation-induced ACh release.

Limitations

In *protocol 1*, because we did not measure the infarct size in the present study, the degree of myocardial protection by hypothermia was undetermined. Whether the reduction of ischemia-induced neurotransmitter release correlates with the reduction of infact size requires further investigations. In *protocols 2* and *3*, baseline NE and ACh levels were not measured. The reduction of stimulation-induced NE and ACh release by hypothermia might be partly due to the reduction of baseline NE and ACh levels. However, because transection of the stellate ganglia (31) or vagi (3) reduces the baseline NE and ACh levels, changes in the baseline NE and ACh levels by hypothermia in *protocols 2* and *3* could not be as large as those observed under innervated conditions in *protocol 1* (Figs. 1 and 2).

In conclusion, hypothermia attenuated the ischemia-induced releases of NE and ACh in the ischemic region to ~30 and 20% of those observed under normothermia, respectively. Hypothermia also attenuated the nerve stimulation-induced releases of NE and ACh to ~70% of those observed during normothermia. In contrast, hypothermia did not affect the decreasing response in the NE level and the increasing response in the ACh level in the nonischemic region, suggesting that the Bezold-Jarisch reflex evoked by the LAD occlusion was maintained.

GRANTS

This study was supported by Health and Labour Sciences Research Grant for Research on Advanced Medical Technology, Health and Labour Sciences Research Grant for Research on Medical Devices for Analyzing, Supporting and Substituting the Function of Human Body, and Health and Labour Sciences Research Grant H18-Iryo-Ippan-023 from the Ministry of Health, Labour and Welfare of Japan; Program for Promotion of Fundamental Studies in Health Science from the National Institute of Biomedical Innovation; a grant provided by the Ichiro Kanehara Foundation; Ground-based Research Announcement for Space Utilization promoted by the Japan Space Forum; and Industrial Technology Research Grant Program 03A47075 from the New Energy and Industrial Technology Development Organization of Japan.

REFERENCES

1. **Akiyama T, Yamazaki T.** Norepinephrine release from cardiac sympathetic nerve endings in the in vivo ischemic region. *J Cardiovasc Pharmacol* 34: S11–S14, 1999.

2. **Akiyama T, Yamazaki T, Ninomiya I.** In vivo monitoring of myocardial interstitial norepinephrine by dialysis technique. *Am J Physiol Heart Circ Physiol* 261: H1643–H1647, 1991.
3. **Akiyama T, Yamazaki T, Ninomiya I.** In vivo detection of endogenous acetylcholine release in cat ventricles. *Am J Physiol Heart Circ Physiol* 266: H854–H860, 1994.
4. **Chernow B, Lake CR, Zaritsky A, Finton CK, Casey L, Rainey TG, Fletcher JR.** Sympathetic nervous system "switch off" with severe hypothermia. *Crit Care Med* 11: 677–680, 1983.
5. **Damsma G, Fibiger HC.** The effects of anaesthesia and hypothermia on interstitial concentrations of acetylcholine and choline in rat striatum. *Life Sci* 48: 2469–2474, 1991.
6. **Duncker DJ, Klassen CL, Ishibashi Y, Herrlinger SH, Pavek T, Bache R.** Effect of temperature on myocardial infarction in swine. *Am J Physiol Heart Circ Physiol* 270: H1189–H1199, 1996.
7. **Genth K, Hofmann M, Hofmann M, Schaper W.** The effect of β-adrenergic blockade on infarct size following experimental coronary occlusion. *Basic Res Cardiol* 76: 144–151, 1981.
8. **Gerevich Z, Tretter L, Adam-Vizi V, Baranyi M, Kiss JP, Zelles T, Vizi ES.** Analysis of high intracellular [Na^+]-induced release of [^{3}H]noradrenaline in rat hippocampal slices. *Neuroscience* 104: 761–768, 2001.
9. **Hale SL, Kloner RA.** Myocardial temperature in acute myocardial infarction: protection with mild regional hypothermia. *Am J Physiol Heart Circ Physiol* 273: H220–H227, 1997.
10. **Jang IK, Van de Werf F, Vanhaecke J, De Geest H.** Coronary reperfusion by thrombolysis and early beta-adrenergic blockade in acute experimental myocardial infarction. *J Am Coll Cardiol* 14: 1816–1823, 1989.
11. **Kakinuma Y, Ando M, Kuwabara M, Katare RG, Okudela K, Kobayashi M, Sato T.** Acetylcholine from vagal stimulation protects cardiomyocytes against ischemia and hypoxia involving additive nonhypoxic induction of HIF-1α. *FEBS Lett* 579: 2111–2118, 2005.
12. **Kao LS, Westhead EW.** Temperature dependence of catecholamine secretion from cultured bovine chromaffin cells. *J Neurochem* 43: 590–592, 1984.
13. **Kawada T, Yamazaki T, Akiyama T, Sato T, Shishido T, Inagaki M, Takaki H, Sugimachi M, Sunagawa K.** Differential acetylcholine release mechanisms in the ischemic and non-ischemic myocardium. *J Mol Cell Cardiol* 32: 405–414, 2000.
14. **Kawada T, Yamazaki T, Akiyama T, Shishido T, Inagaki M, Uemura K, Miyamoto T, Sugimachi M, Takaki H, Sunagawa K.** In vivo assessment of acetylcholine-releasing function at cardiac vagal nerve terminals. *Am J Physiol Heart Circ Physiol* 281: H139–H145, 2001.
15. **Kitagawa H, Akiyama T, Yamazaki T.** Effects of moderate hypothermia on in situ cardiac sympathetic nerve endings. *Neurochem Int* 40: 235–242, 2002.
16. **Kitagawa H, Yamazaki T, Akiyama T, Mori H, Sunagawa K.** Effects of moderate hypothermia on norepinephrine release evoked by ouabain, tyramine and cyanide. *J Cardiovasc Pharmacol* 41: S111–S114, 2003.
17. **Ku DD, Lucchesi BR.** Effects of dimethyl propranolol (UM-272; SC-27761) on myocardial ischemic injury in the canine heart after temporary coronary artery occlusion. *Circulation* 57: 541–548, 1978.
18. **Kurz T, Richardt G, Hagl S, Seyfarth M, Schömig A.** Two different mechanisms of noradrenaline release during normoxia and simulated ischemia in human cardiac tissue. *J Mol Cell Cardiol* 27: 1161–1172, 1995.
19. **Lameris TW, de Zeeuw S, Alberts G, Boomsma F, Duncker DJ, Verdouw PD, Veld AJ, van den Meiracker AH.** Time course and mechanism of myocardial catecholamine release during transient ischemia in vivo. *Circulation* 101: 2645–2650, 2000.
20. **Lameris TW, de Zeeuw S, Duncker DJ, Alberts G, Boomsma F, Verdouw PD, van den Meiracker AH.** Exogenous angiotensin II does not facilitate norepinephrine release in the heart. *Hypertension* 40: 491–497, 2002.
21. **Maxwell MP, Hearse DJ, Yellon DM.** Species variation in the coronary collateral circulation during regional myocardial ischaemia: a critical determinant of the rate of evolution and extent of myocardial infarction. *Cardiovasc Res* 21: 737–746, 1987.
22. **Rona G.** Catecholamine cardiotoxicity. *J Mol Cell Cardiol* 17: 291–306, 1985.
23. **Schwartz JH.** Neurotransmitters. In: *Principles of Neural Science* (4th Ed.), edited by Kandel ER, Schwartz JH, Jessell TM. New York: McGraw-Hill, 2000, p. 280–297.
24. **Schömig A, Kurz T, Richardt G, Schömig E.** Neuronal sodium homeostasis and axoplasmic amine concentration determine calcium-independent noradrenaline release in normoxic and ischemic rat heart. *Circ Res* 63: 214–226, 1988.
25. **Simkhovich BZ, Hale SL, Kloner RA.** Metabolic mechanism by which mild regional hypothermia preserves ischemic tissue. *J Cardiovasc Pharmacol Ther* 9: 83–90, 2004.
26. **Toombs CF, Wiltse AL, Shebuski RJ.** Ischemic preconditioning fails to limit infarct size in reserpinized rabbit myocardium. Implication of norepinephrine release in the preconditioning effect. *Circulation* 88: 2351–2358, 1993.
27. **Torr S, Drake-Holland AJ, Main M, Hynd J, Isted K, Noble MIM.** Effects on infarct size of reperfusion and pretreatment with β-blockade and calcium antagonists. *Basic Res Cardiol* 84: 564–582, 1989.
28. **Van den Doel MA, Gho BC, Duval SY, Schoemaker RG, Duncker DJ, Verdouw PD.** Hypothermia extends the cardioprotection by ischaemic preconditioning to coronary artery occlusions of longer duration. *Cardiovasc Res* 37: 76–81, 1998.
29. **Vander Heide RS, Schwartz LM, Jennings RB, Reimer KA.** Effect of catecholamine depletion on myocardial infarct size in dogs: role of catecholamines in ischemic preconditioning. *Cardiovasc Res* 30: 656–662, 1995.
30. **Vizi ES.** Different temperature dependence of carrier-mediated (cytoplasmic) and stimulus-evoked (exocytotic) release of transmitter: a simple method to separate the two types of release. *Neurochem Int* 33: 359–366, 1998.
31. **Yamazaki T, Akiyama T, Kitagawa H, Takauchi Y, Kawada T, Sunagawa K.** A new, concise dialysis approach to assessment of cardiac sympathetic nerve terminal abnormalities. *Am J Physiol Heart Circ Physiol* 272: H1182–H1187, 1997.
32. **Zheng F, Kidd C, Bowser-Riley F.** Effects of moderate hypothermia on baroreflex and pulmonary chemoreflex heart rate response in decerebrate ferrets. *Exp Physiol* 81: 409–420, 1996.

REGULAR PAPER

J. Physiol. Sci. Vol. 56, No. 5; Oct. 2006; pp. 325–333
Online Sep. 9, 2006; **doi:10.2170/physiolsci.RP009006**

Baroreflex Increases Correlation and Coherence of Muscle Sympathetic Nerve Activity (SNA) with Renal and Cardiac SNAs

Atsunori KAMIYA, Toru KAWADA, Masaki MIZUNO, Tadayoshi MIYAMOTO, Kazunori UEMURA, Kenjiro SEKI, Shuji SHIMIZU, and Masaru SUGIMACHI

Department of Cardiovascular Dynamics, National Cardiovascular Centre Research Institute, Osaka, 565-8565 Japan

Abstract: Despite accumulating data of muscle sympathetic nerve activity (SNA) measured by human microneurography, whether neural discharges of muscle SNA correlates and coheres with those of other SNAs controlling visceral organs remains unclear. Further, how the baroreflex control of SNA affects the relations between these SNAs remains unknown. In urethane and α-chloralose anesthetized, vagotomized, and aortic-denervated rabbits, we recorded muscle SNA from the tibial nerve using microneurography and simultaneously recorded renal and cardiac SNAs. After isolating the carotid sinuses, we produced a baroreflex closed-loop condition by matching the isolated intracarotid sinus pressure (CSP) with systemic arterial pressure (CLOSE). We also fixed CSP at operating pressure (FIX) or altered CSP widely (WIDE: operating pressure ± 40 mmHg). Under these conditions, we calculated time-domain and frequency-domain measures of the correlation between muscle SNA and renal or cardiac SNAs. At CLOSE, muscle SNA resampled at 1 Hz correlated with both renal ($r^2 = 0.71 \pm 0.04$, delay = 0.10 ± 0.004 s) and cardiac SNAs ($r^2 = 0.58 \pm 0.03$, delay = 0.13 ± 0.004 s) at optimal delays. Moreover,muscle SNA at CLOSE strongly cohered with renal and cardiac SNAs(coherence >0.8) at the autospectral peak frequencies, and weakly (0.4–0.5) at the remaining frequencies. Increasing the magnitude of CSP change from FIX to CLOSE and further to WIDE resulted in corresponding increases in correlation and coherence functions at nonpeak frequencies, and the coherence functions at peak frequencies remained high (>0.8). In conclusion, muscle SNA correlates and coheres approximately with renal and cardiac SNAs under closed-loop baroreflex conditions. The arterial baroreflex is capable of potently homogenizing neural discharges of these SNAs by modulating SNA at the nonpeak frequencies of SNA autospectra.

Key words: sympathetic nerve activity, muscle, baroreflex.

Sympathetic nerve activity (SNA) has the crucial role of controlling circulation [1] and thus has been a major target in the research of circulatory physiology and pathophysiology. In humans, microneurography is the only direct method to measure SNA discharge [2]. By this technique, numerous human studies measured the activity of sympathetic nerves innervating the blood vessels in skeletal muscles (muscle SNA) [2–5] and used it as systemic SNA [3, 6–10]. However, since the measurable region in humans by this technique is almost limited to upper and lower extremities [2], the relation between muscle SNA and the SNAs controlling visceral organs such as the kidney and heart is not fully understood.

Arterial baroreflex is a major controller of SNA and thus may affect the relations between these SNAs. We previously reported that static-nonlinear and dynamic-linear baroreflex control of muscle SNA is similar to that of renal and cardiac SNAs under physiological pressure change in rabbits [11, 12]. Consistent with this finding, we have indeed observed that muscle SNA averaged over 1 minute parallels renal and cardiac SNAs in response to forced baroreceptor pressure change [11]. However, the relation between these SNAs in a time domain faster than 1 min and the relation in frequency domain remain unknown, despite the importance of their physiological and clinical relevance. First, the relation between these SNAs under conditions in which arterial pressure is regulated to normal level by a closed-loop baroreflex system is unclear. Next, the effects of baroreflex on the homogeneity in SNAs have not been analyzed quantitatively. Although canceling and enlarging the changes in baroreceptor pressure under open-loop baroreflex conditions are speculated to decrease and increase the homogeneity, respectively, how much muscle SNA correlates and coheres with other SNAs under these conditions remains unknown.

In the present study, we tested two hypotheses: (i) muscle SNA correlates and coheres with renal and cardiac SNAs under a closed-loop baroreflex condition, and (ii) the arterial baroreflex is capable of homogenizing neural discharges of these SNAs. In anesthetized rabbits with ca-

Received on Jul 27, 2006; accepted on Sep 6, 2006; released online on Sep 9, 2006; doi:10.2170/physiolsci.RP009006
Correspondence should be addressed to: Atsunori Kamiya, Department of Cardiovascular Dynamics, National Cardiovascular Centre Research Institute, Osaka 565-8565, Japan. Tel: +81-6-6833-5012; Fax: +81-6-6835-5403; E-mail: kamiya@ri.ncvc.go.jp

rotid sinuses isolated from systemic circulation, we simultaneously recorded muscle SNA from the tibial nerve by microneurography as well as renal and cardiac SNAs. We investigated the relation of muscle SNA with renal and cardiac SNAs under closed-loop baroreflex conditions and determined the proportions of the variance components of muscle SNA correlating and not correlating with renal and cardiac SNAs. Further, we also investigated these relations under two open-loop baroreflex conditions: fixed and widely fluctuating baroreceptor pressure.

MATERIALS AND METHODS

Surgical preparations. The animals were cared for in strict accordance with the Guiding Principles for the Care and Use of Animals in the Field of Physiological Sciences approved by the Physiological Society of Japan. Ten Japanese white rabbits weighing 2.4–3.3 kg were anesthetized by intravenous injection (2 ml/kg) of a mixture of urethane (250 mg/ml) and α-chloralose (40 mg/ml) and mechanically ventilated with oxygen-enriched room air. Supplemental anesthetics were injected as necessary (0.5 ml/kg) to maintain an appropriate level of anesthesia. We isolated the bilateral carotid sinuses vascularly from the systemic circulation by ligating the internal and external carotid arteries and other small branches originating from the carotid sinus regions. The isolated carotid sinuses were filled with warmed physiological saline through catheters inserted via the common carotid arteries. The intracarotid sinus pressure (CSP) was controlled by a servo-controlled piston pump (model ET-126A, Labworks; Costa Mesa, CA). Bilateral vagal and aortic depressor nerves were sectioned at the midlevel of the neck to eliminate baroreflexes from the cardiopulmonary region and the aortic arch. The systemic arterial pressure (AP) was measured using a high-fidelity pressure transducer (Millar Instruments; Houston, TX) inserted retrograde from the right common carotid artery below the isolated carotid sinus region. Body temperature was maintained at approximately 38°C with a heating pad.

We exposed the left renal sympathetic nerve retroperitoneally and the left cardiac sympathetic nerve through a middle thoracotomy. We attached a pair of stainless steel wire electrodes (Bioflex wire AS633, Cooner Wire) to each of these nerves to record renal and cardiac SNAs. To eliminate afferent signals, we tightly ligated and crushed the nerve fibers peripheral to the electrodes. To insulate and fix the electrodes, we covered the nerve and electrodes with a mixture of silicone gel (Silicon Low Viscosity, KWIK-SIL, World Precision Instrument, Inc., FL). We band-pass filtered the preamplified nerve signals at 150–1,000 Hz.

We exposed the left tibial nerve at the right popliteal fossa by incising the flexors of the dorsal middle thigh. We inserted a tungsten microelectrode (model 26-05-1, Federick Haer and Co., Bowdoinham, ME) to the right tibial nerve to record muscle SNA according to the microneurographic technique reported in humans [2, 13] and animals [14]. We identified muscle SNA according to the following discharge characteristics: (i) afferent activity being induced by tapping of the calf muscles but not by gently touching the skin, and (ii) excitatory and inhibitory responses to decreasing and increasing CSP, respectively. Then we tightly ligated and crushed the nerve fibers peripheral to the electrodes to eliminate afferent signals from the muscles. We fed the nerve signals into a preamplifier (Kohno Instruments, Nagoya) with active band-pass filters set from 480 to 5,000 Hz and continuously monitored these signals through a sound speaker.

We full-wave rectified and low-pass filtered the SNA signals with a cutoff frequency of 30 Hz to quantify the nerve activity. Pancuronium bromide (0.1 mg/kg) was administrated to prevent a contamination of muscular activity in these SNA recordings.

Protocols. After the surgical preparation, we kept the animal horizontally in a supine position. To test the first hypothesis that a neural discharge of muscle SNA parallels that of renal and cardiac SNAs, we measured the three SNAs while closing the baroreflex negative feedback loop by matching CSP with systemic AP (CLOSE protocol). We recorded CSP, SNAs, and systemic AP for 15 min at a sampling rate of 200 Hz, using a 12-bit analog-to-digital converter. After stabilizing the condition for at least 5 min, we recorded the data for 10 min and stored them on the hard disk of a dedicated laboratory computer system for later analysis. We also calculated the actual operating pressure by averaging systemic AP from the data.

To test the second hypothesis that baroreflex contributes to homogeneous sympathetic activation, we eliminated and greatly widened the baroreceptor pressure changes by the FIX and WIDE protocols, respectively, in baroreflex open-loop conditions. In the FIX protocol, we fixed CSP at the operating pressure [15, 16]. In the WIDE protocol, we randomly assigned CSP at 40 mmHg either above or below the operating pressure every 500 ms according to a binary white noise sequence [15, 17], where the input power spectrum of CSP was reasonably flat up to 1 Hz. The FIX and WIDE protocols were conducted serially in a randomized order at intervals of at least 5 min between protocols. During each protocol, we recorded measurements for 10 min and stored the data for analysis.

Data analysis. Under each baroreceptor pressure condition of CLOSE, WIDE, and FIX, we calculated the time domain (correlation coefficient) and frequency domain measures (coherence function) between muscle and renal or cardiac SNAs. In the time-domain analysis, we resampled SNA data at 1 Hz, assigned 100 arbitrary units (a.u.) to the maximal value during 10 min of CLOSE, and normalized other SNA signals to this value.

We scatter-plotted muscle SNA at 1 Hz against renal and cardiac SNAs with variable delays from renal and cardiac SNAs to muscle SNA (range: from 0 to 0.30 s at increments of 0.01 s) and calculated the correlation coefficient (r) [18] with optimal delays that maximized the square of correlation coefficient (r^2). The delays reflected the distances from the brain to the sites of measurement of these SNAs. The r^2 shows how perfectly a linear regression line describes the relationship between the two SNAs [19].

We also calculated the variance of muscle SNA resampled at 1 Hz [19]. The variance may include two components, one that correlates (correlative variance) and the other that does not correlate (noncorrelative variance) with other SNAs. Therefore we defined correlative and noncorrelative variance of muscle SNA to renal or cardiac SNA as follows (see APPENDIX) [18, 19]:

Correlative variance = SNA variance·r^2
Noncorrelative variance = SNA variance·$(1 - r^2)$

where SNA variance was the variance of muscle SNA, and r^2 was the correlation coefficient of muscle SNA against renal or cardiac SNA.

In the frequency-domain analysis, we calculated the coherence functions between muscle SNA and renal or cardiac SNA. We resampled SNA data at 10 Hz, and segmented them into 10 sets of 50% overlapping bins of 2^{10} data point each. SNA signals were similarly normalized as mentioned above. The segment length was 102.4 s, which yields the lowest frequency bound of 0.01 (0.0097) Hz. For each data set, we performed a fast Fourier transform while subtracting a linear trend and applying a Hanning window for each segment. We performed fast Fourier transform and ensemble averaged the power of muscle SNA [$S_{xx}(f)$], the power of renal or cardiac SNA [$S_{yy}(f)$], and the cross power between muscle SNA and renal or cardiac SNA [$S_{yx}(f)$] over the 10 segments. We derived a magnitude-squared coherence function [$Coh(f)$] of muscle SNA versus renal and cardiac SNAs as follows [17]:

$$Coh(f) = \frac{|S_{yx}(f)|^2}{S_{xx}(f)S_{yy}(f)}$$

The coherence value ranges from zero to unity. Unity coherence indicates a perfect linear correlation between muscle SNA and other SNAs, whereas zero coherence indicates total independence of the two SNAs. In an SNA autospectrum, when the power was three times greater than the averaged power of SNA from 0.01 to 1 Hz, we defined it as a peak. We separately calculated the averaged coherence function at the peak frequencies of muscle SNA autospectra and that at the remaining frequencies.

Statistic analysis. We presented all data as means ± SD. We used a repeated-measures analysis of variance with post hoc multiple comparisons to compare variables among experimental baroreceptor pressure conditions (FIX, CLOSE, WIDE) [19]. We considered differences significant when $P < 0.05$.

RESULTS

Relation between muscle SNA and cardiac or renal SNA in closed-loop baroreflex condition of CLOSE protocol

Time-domain analysis. In the CLOSE protocol (CSP matched with systemic arterial pressure), typical neural discharges of muscle SNA at 10 Hz appeared roughly the same as those of renal and cardiac SNAs (Fig. 1A). When the delay from renal and cardiac SNAs to muscle SNA was determined in individual animals to maximize r^2 (a typical example is shown in Fig. 1), muscle SNA resampled at 1 Hz correlated with both renal and cardiac SNAs with r^2 of 0.81 (delay = 0.10 s) and 0.64 (delay = 0.13 s), respectively (Fig. 1, B and C). The averaged data of all animals also showed that muscle SNA correlated with renal SNA ($r^2 = 0.71 \pm 0.04$, delay = 0.10 ± 0.004 s) and with

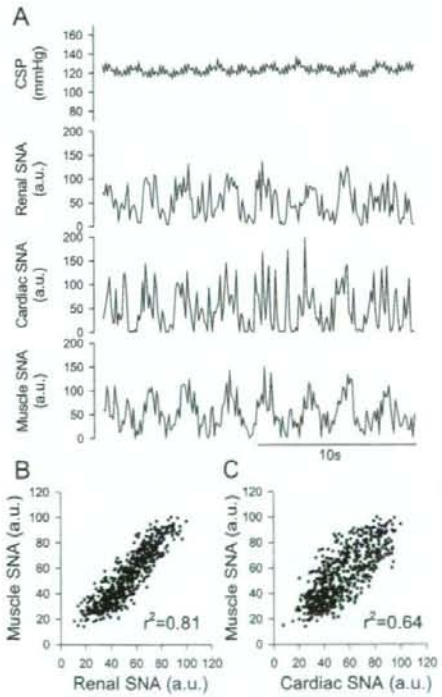

Fig. 1. (**A**) Representative time series for CSP, renal, cardiac, and muscle SNAs resampled at 10 Hz under the baroreflex closed-loop condition of CLOSE (CSP was matched to systemic AP). (**B**) Scatter plot of muscle SNA against renal SNA. (**C**) Scatter plot of muscle SNA against cardiac SNAs. The SNA signals were further resampled at 1 Hz. The delay from renal (0.10 s) or cardiac SNA (0.13 s) to muscle SNA was determined as the value that maximized r^2.

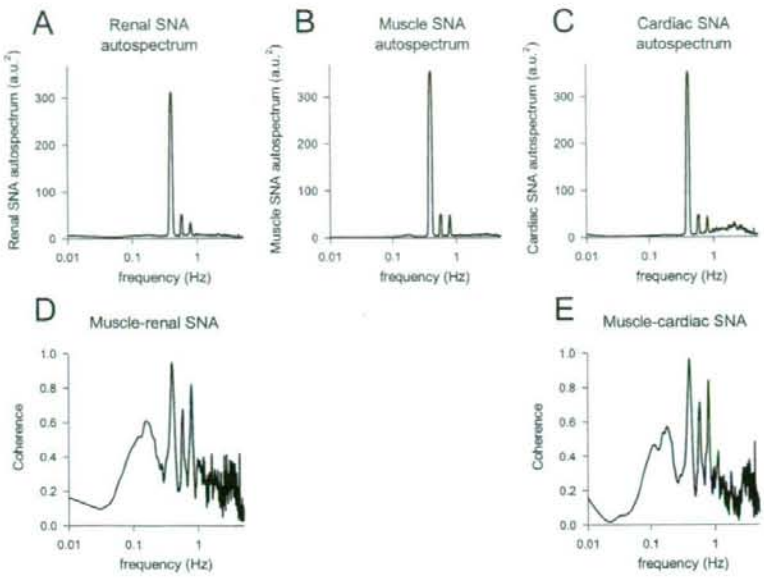

Fig. 2. Autospectra of renal (**A**), muscle (**B**), and cardiac SNAs (**C**) resampled at 1 Hz, and the coherence function of muscle SNA against renal (**D**) and cardiac SNAs (**E**) under the baroreflex closed-loop condition of CLOSE (CSP was matched to systemic AP), using the same data as in Fig. 1.

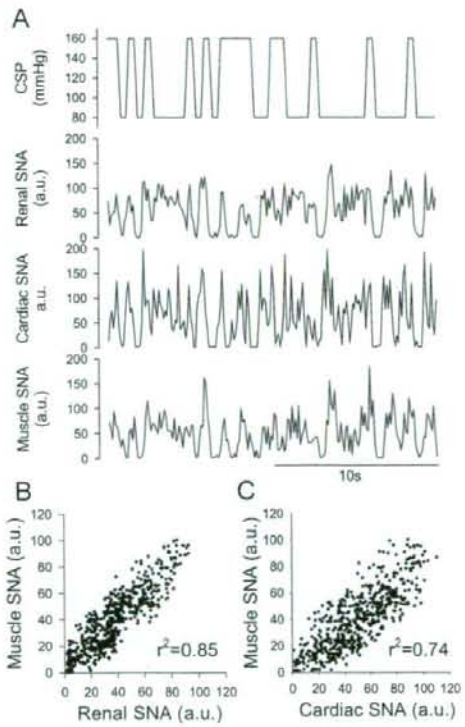

Fig. 3. (**A**) Representative time series for CSP, renal, cardiac, and muscle SNAs resampled at 10 Hz under the baroreflex open-loop condition of WIDE (CSP was varied according to a binary white noise sequence at 40 mmHg either above or below the operating pressure). (**B**) Scatter plots of muscle SNA resampled at 1 Hz against renal SNA (delay = 0.10 s). (**C**) Scatter plots of muscle SNA resampled at 1 Hz against cardiac SNA (delay = 0.13 s).

cardiac SNA ($r^2 = 0.58 \pm 0.03$, delay = 0.13 ± 0.004 s) (Fig. 5, A and B). The r^2 was greater with renal than with cardiac SNA ($P < 0.05$). The pulse pressure of CSP was 30–40 mmHg.

Frequency-domain analysis. In the same animal as in Fig. 1, the autospectra of these SNAs showed a few peaks at common frequency ranges (Fig. 2, A, B, and C). Muscle SNA cohered with both renal and cardiac SNAs strongly at the peak frequencies of muscle SNA autospectra, but weakly at the remaining frequencies (Fig. 2, D and E). The individual animals all showed similar characteristics. The averaged coherence function of the animals was strong at the peak frequencies of the muscle SNA autospectrum (0.93 ± 0.01 between muscle and renal SNAs and 0.87 ± 0.02 between muscle and cardiac SNAs), but was weak at the remaining frequencies (0.5) (Fig. 8).

Effects of the magnitude of change in baroreceptor pressure on the relation between muscle SNA and cardiac or renal SNA

Time-domain analysis. In the same animal as in Fig. 1, the pattern of neural discharge of muscle SNA at 10 Hz resembled those of renal and cardiac SNAs to a greater extent in the WIDE protocol (CPS fluctuating between operating pressure ± 40 mmHg) (Fig. 3) than in the FIX protocol (CPS fixed at operating pressure) (Fig. 4). The correlation of muscle SNA resampled at 1 Hz with renal and cardiac SNAs was higher in WIDE ($r^2 = 0.85$, delay = 0.10 s, and $r^2 = 0.74$, delay = 0.13 s, respectively) (Fig. 3, B and C) than in CLOSE, but was lower in FIX (with the same delays, Fig. 4, B and C). Compared with CLOSE, the averaged data of all animals showed a higher correlation of muscle SNA with renal and cardiac SNAs in WIDE ($r^2 = 0.79 \pm 0.03$, delay = 0.10 ± 0.004 s, and r^2 =

0.76 ± 0.02, delay = 0.13 ± 0.004 s, respectively), but lower correlation in FIX (r^2 = 0.53 ± 0.04, delay = 0.10 ± 0.004 s, and r^2 = 0.46 ± 0.04, delay = 0.13 ± 0.004 s, respectively) (Fig. 5, A and B). In WIDE, the r^2 was higher with renal than with cardiac SNA ($P < 0.05$). Similar results were observed when SNAs were resampled at slower and faster frequencies than 1 Hz (Fig. 6). In both SNA pairs, the r^2 was greater in WIDE than in CLOSE and FIX at frequencies from 0.01 to 5 Hz ($P < 0.05$), whereas it was greater in CLOSE than in FIX at frequencies from 0.3 to 5 Hz ($P < 0.05$).

The variance of muscle SNA sampled at 1 Hz increased from FIX to CLOSE and further to WIDE (Fig. 5, C and D; gray plus black column). The variance component of

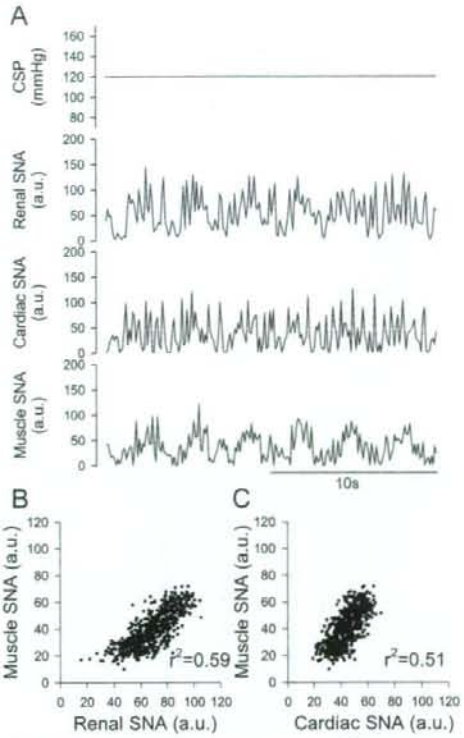

Fig. 4. (**A**) Representative time series for CSP, renal, cardiac, and muscle SNAs resampled at 10 Hz under the baroreflex open-loop condition of FIX (CSP was fixed at the operating pressure). (**B**) Scatter plot of muscle SNA resampled at 1 Hz against renal SNA (delay = 0.10 s). (**C**) Scatter plots of muscle SNA resampled at 1 Hz against cardiac SNA (delay = 0.13 s).

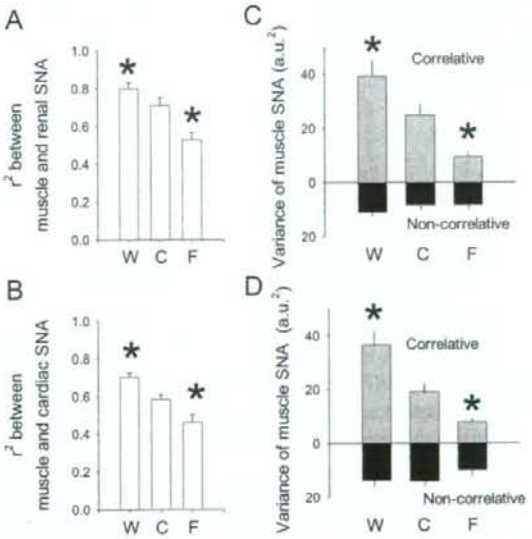

Fig. 5. The square of correlation coefficient (r^2) between muscle SNA resampled at 1 Hz and renal (**A**) or cardiac SNA (**B**) under baroreceptor pressure conditions of WIDE, CLOSE, and FIX. Floating columns show the averaged (±SD) correlative (gray top column) and noncorrelative (black bottom column) variance of muscle SNA versus renal (**C**) or cardiac SNA (**D**) resampled at 1 Hz in WIDE, CLOSE, and FIX. Correlative: variance component of muscle SNA correlating with other SNA; Noncorrelative: variance component of muscle SNA not correlating with other SNA; W: WIDE; C: CLOSE; F: FIX. *: $P < 0.05$, vs. CLOSE.

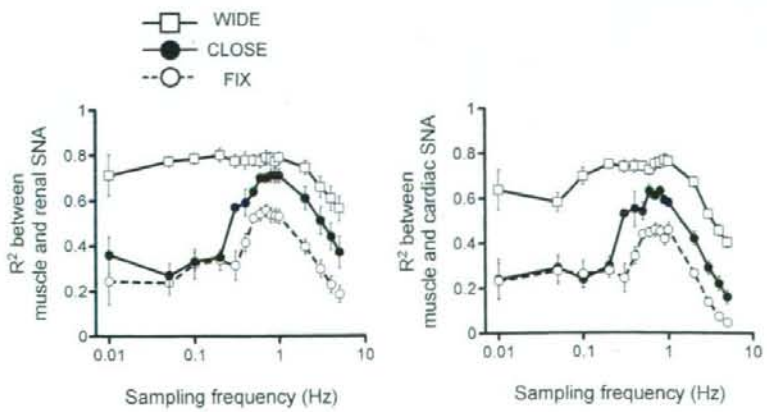

Fig. 6. The square of correlation coefficient (r^2) over SNA sampling frequency (0.01–5.0 Hz) between muscle SNA and renal (**A**) or cardiac SNA (**B**) under baroreceptor pressure conditions of WIDE (open square), CLOSE (closed circle), and FIX (open circle). In both SNA pairs, the r^2 was greater in WIDE than in CLOSE and FIX at frequencies observed ($P < 0.05$), whereas it was greater in CLOSE than in FIX at frequencies from 0.3 to 5.0 Hz ($P < 0.05$).

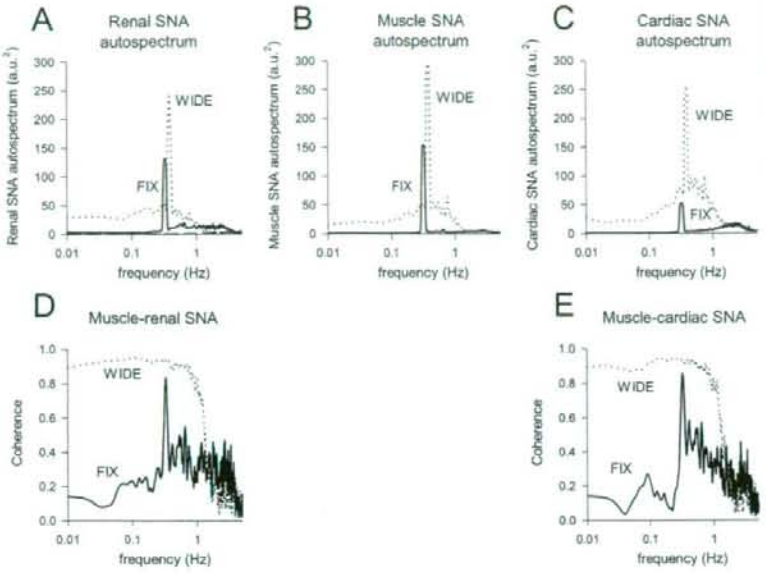

Fig. 7. Autospectra of renal (**A**), muscle (**B**), and cardiac SNAs (**C**), and the coherence function of muscle SNA against renal (**D**) and cardiac SNAs (**E**) under baroreflex open-loop conditions of WIDE (broken line) and FIX (solid line), using the same data as in Figs. 3 and 4.

muscle SNA that correlates with other SNAs, calculated as muscle SNA variance·r^2 ranked in the order of WIDE > CLOSE > FIX (Fig. 5, C and D; gray column), indicating a contribution of baroreflex-dependent regulation in maintaining homogeneity between muscle SNA and other visceral SNAs. In contrast, the variance component of muscle SNA that does not correlate with other SNAs, calculated as variance · $(1 - r^2)$, was similar among FIX, CLOSE, and WIDE (Fig. 5, C, D; black bottom column).

Frequency-domain analysis. In the same animal as in Fig. 1, the autospectra of muscle, renal, and cardiac SNAs peaked at exactly the same frequencies both in the WIDE and FIX protocols (Fig. 7, A, B, and C). Muscle SNA strongly cohered with both renal and cardiac SNAs both in WIDE and FIX at peak frequencies of the muscle SNA autospectra; however, the correlation was strong in WIDE but weak in FIX at the remaining frequencies (Fig. 7, D and E). The data of individual animals showed similar characteristics. The averaged coherence functions of all animals was consistently strong (>0.8) at peak frequencies of the muscle SNA autospectra regardless of baroreceptor pressure conditions of WIDE, CLOSE, and FIX (Fig. 8, black column). In contrast, the averaged coherence functions at the remaining frequencies were higher in WIDE (>0.8) compared with CLOSE or FIX (0.4–0.5) (Fig. 8, gray column).

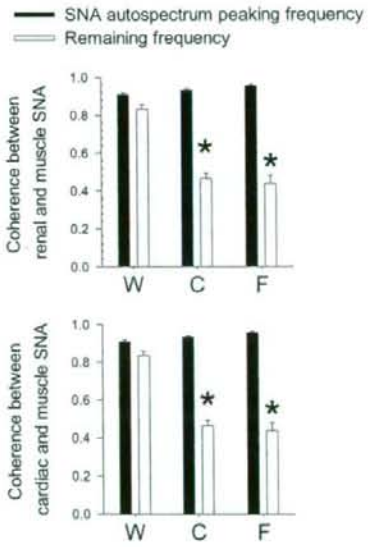

Fig. 8. Averaged coherence functions of muscle SNA against renal and cardiac SNAs at muscle SNA autospectral peak frequencies (black column) and at the remaining frequencies (gray column) under baroreceptor pressure conditions of WIDE, CLOSE, and FIX. W: WIDE; C: CLOSE; F: FIX. *P < 0.05, WIDE vs. CLOSE and FIX.

DISCUSSION

Despite the accumulating data on muscle SNA measured by microneurography in human studies, whether the neural discharge of muscle SNA correlates and coheres with that of other SNAs controlling visceral organs remains unclear. The major new findings in this study are (i) under the baroreflex closed-loop condition when CSP is matched with the systemic arterial pressure (CLOSE), muscle SNA resampled at 1 Hz correlates with both renal and cardiac SNAs in time-domain analysis (r^2: 0.6–0.7, with proper delay), and (ii) muscle SNA coheres with renal and cardiac SNAs in frequency domain analysis, particularly at peak frequencies of the SNA autospectra.

These results support our first hypothesis and indicate that muscle SNA correlates and coheres approximately with renal and cardiac SNAs under closed-loop baroreflex condition.

Next, although the baroreflex is known to strongly regulate muscles [3], renal and cardiac SNA [15, 20], the contribution of baroreflex to the homogeneous SNA discharges has not been elucidated quantitatively. The other major new findings in this study are as follows. When the change in baroreceptor pressure is increased from FIX (fixed CSP, no change) to CLOSE (CSP matching systemic arterial pressure, pulse pressure 30–40 mmHg) and further to WIDE (CSP fluctuating between ±40 mmHg), there are corresponding increases in the time domain correlation (r^2) of muscle SNA resampled at 1 Hz with renal and cardiac SNAs, from approximately 0.5 (FIX), to 0.6–0.7 (CLOSE), and to 0.8 (WIDE) (Fig. 5, A and B). The baroreflex dependent characteristics were also observed when SNAs were resampled at a frequency from 0.3 to 5.0 Hz (Fig. 6). This is also consistent with increases in the variance component of muscle SNA correlating with renal and cardiac SNAs (Fig. 5, C and D). These results agree with the concept that the baroreflex is important in generating harmonized SNA discharges [5, 21]. Moreover, the results indicate that arterial baroreflex has the ability to increase the homogeneity between these SNAs by nearly twofold. They support our second hypothesis and indicate that the arterial baroreflex potently homogenizes neural discharges of these SNAs.

Our results indicate that baroreflex increases the homogeneity between these SNAs by modulating SNA at nonpeak frequencies of SNA autospectra. The frequency domain correlation (coherence function) of muscle SNA with renal and cardiac SNAs was increased from approximately 0.4–0.5 (FIX), to 0.5 (CLOSE), to 0.9 (WIDE) at nonpeak frequencies, not peaking frequencies, of the SNA autospectra (Fig. 8). This suggests that other mechanisms other than baroreflex govern SNA at the nonpeak frequencies.

Our results quantitatively indicate that baroreflex-independent factors contribute to one-half of the homogeneity between muscle SNA and cardiac or renal SNA. Time-domain data show that even under a condition in which CSP is fixed at operating pressure, one-half of the variance of muscle SNAs correlates with other SNAs (Fig. 5, C and D; gray top column), with r^2 of approximately 0.5 (Fig. 5, A and B). These data indicate the presence of a baroreflex-independent component of SNA homogeneity. Although some noises may be included in the variance component of muscle SNA correlating with other SNAs, this is negligible in the calculation of variance, since the signal/noise ratio in SNA is >1,000 (noise was measured as the signal obtained after an individual animal died). The baroreflex-independent component of SNA homogeneity may be related to the strong coherence function between the SNAs at autospectral peak frequencies, since the coherence is consistently high regardless of the magnitude of baroreceptor pressure changes (Figs. 7, D and E, and 8). This component may partially be associated with the respiratory-related rhythm in sympathetic nerve discharge, a concept of central respiratory rhythm generator [21–23]. At the autospectral peak frequencies, these mechanisms may keep the coherence sufficiently high (0.9) independent of the baroreflex, and thus the baroreflex cannot increase the coherence further.

In contrast to the homogeneous sympathetic activation, the heterogeneity of muscle SNA versus renal or cardiac SNA does not relate with baroreflex. The proportions of the variance component of muscle SNA not correlating with renal and cardiac SNAs are constant regardless of the magnitude of change in baroreceptor pressure (Fig. 5, C and D). Mechanisms other than baroreflex may be involved in heterogeneous sympathetic activation. For example, chemoreflex [24], nitric oxide synthesis [25], and osmolarity [26] have been reported to produce regional differences in sympathetic activations.

Our data may strengthen the interpretation and the impact of the accumulated data on the involvement of human muscle SNA in circulatory physiology [3, 6–8, 10] and cardiovascular diseases [27, 28]. The recording of human microneurography is limited to the limbs, and there is so far little direct experimental evidence to support that muscle SNA parallel the other SNAs controlling visceral organs. The present study addresses this issue as an initial step and demonstrates the similarity between muscle SNA discharge and renal or cardiac SNA. Further study is needed to investigate the relations between SNAs in response to stimuli other than baroreflex.

Earlier studies have reported the coherence between pairs of SNA discharges for cardiac, renal, splanchnic, splenic, and lumbar SNAs in animals [29–31]. However, most of the studies focused on the coherence at frequencies faster than 1 Hz (0–15 Hz), in contrast to the present study. Furthermore, the previous studies did not measure muscle SNA or quantitatively investigate the effects of baroreflex on homogeneous SNA discharges.

Limitations

The present study has several limitations. First, anesthetic agents tend to inhibit efferent SNA and depress the gain of baroreflex control of SNA. Second, we excluded the efferent vagal nerve activities, which could affect SNA and baroreflex. Third, artificial respiration and surgical procedures used in this study may affect SNA and baroreflex. Last, based on most of the frequency domain studies of human muscle SNA [32–35], we focused on sympathetic discharge at frequencies of up to 1 Hz. And because of the low-pass characteristics of transfer function from SNA to arterial pressure (baroreflex peripheral arc) [20], the dynamic property of pressure response to

SNA becomes smaller as the frequency of SNA discharge increases. Future studies are needed to investigate the relation of muscle SNA with other SNAs at faster SNA rhythms, including a cardiac-related SNA rhythm at a frequency of 2 to 6 Hz [36] and an SNA rhythm of 10 Hz [37].

In conclusion, 1-Hz muscle SNA correlated with both renal and cardiac SNAs in time-domain analysis and cohered with renal and cardiac SNAs in frequency-domain analysis. Accompanying an increase in the magnitude of baroreceptor pressure change, both the correlation coefficient and the coherence function increased. These results indicate that muscle SNA correlates and coheres approximately with renal and cardiac SNAs under the closed-loop baroreflex condition and that the arterial baroreflex is capable of potently homogenizing neural discharges of these SNAs by modulating SNA at nonpeak frequencies of SNA autospectra.

APPENDIX

When y is scatter-plotted against x, a linear regression line can be drawn between the two variables. The Pearson product-moment correlation coefficient (r) between variables has the following relationship with variance (Eq. 1) [19]

$$r^2 = 1 - \frac{SS_{res}}{V_y} \quad (1)$$

where SS_{res} is the sum of squared deviations (residuals) from the regression line and V_y is the total sum of squared deviations from the mean of the dependent variable (y), that is, the total variance of y.

Equation 1 indicates that the square of correlation coefficient, r^2, is a fraction of the total variance in the dependent variable (y), which is explained by a linear regression relation [18, 19]. Equation 1 leads to the following relations in Eqs. 2 and 3.

$$V_y \cdot r^2 + SS_{res} = V_y \quad (2)$$

$$SS_{res} = V_y \cdot (1 - r^2) \quad (3)$$

$V_y \cdot r^2$ indicates the component of total variance in y that is explained by a linear regression relation (correlative variance in y). SS_{res} indicates the residual component of total variance in y that is not explained by linear regression relation (noncorrelative variance in y).

This study was supported by the Ground-based Research Announcement for Space Utilization project promoted by the Japan Space Forum, the research project promoted by the Ministry of Health, Labour and Welfare in Japan (#H18-nano-ippan-003), and the Grants-in-Aid for Scientific Research promoted by the Ministry of Education, Culture, Sports, Science and Technology in Japan (#18591992).

REFERENCES

1. Rowell LB. Human cardiovascular control. New York: Oxford Univ. Press; 1993.
2. Mano T. Microneurography as a tool to investigate sympathetic nerve responses to environmental stress. Aviakosmicheskaia i Ekologicheskaia Meditsina. 1997;31:8-14.
3. Wallin BG, Eckberg DL. Sympathetic transients caused by abrupt alterations of carotid baroreceptor activity in humans. Am J Physiol. 1982;242:H185-90.
4. Wallin BG, Esler M, Dorward P, Eisenhofer G, Ferrier C, Westerman R, *et al.* Simultaneous measurements of cardiac noradrenaline spillover and sympathetic outflow to skeletal muscle in humans. J Physiol (Lond). 1992;453:45-58.
5. Wallin BG, Thompson JM, Jennings GL, Esler MD. Renal noradrenaline spillover correlates with muscle sympathetic activity in humans. J Physiol (Lond). 1996;491:881-7.
6. Kamiya A, Michikami D, Fu Q, Niimi Y, Iwase S, Mano T, *et al.* Static handgrip exercise modifies arterial baroreflex control of vascular sympathetic outflow in humans. Am J Physiol Regul Integr Comp Physiol. 2001;281:R1134-9.
7. Markel TA, Daley JC, 3rd, Hogeman CS, Herr MD, Khan MH, Gray KS, *et al.* Aging and the exercise pressor reflex in humans. Circulation. 2003;107:675-8.
8. Mitchell JH, Victor RG. Neural control of the cardiovascular system: insights from muscle sympathetic nerve recordings in humans. Med Sci Sports Exerc. 1996;28(10 Suppl):S60-9.
9. Mosqueda-Garcia R, Furlan R, Tank J, Fernandez-Violante R. The elusive pathophysiology of neurally mediated syncope. Circulation. 2000;102:2898-906.
10. Tank J, Schroeder C, Diedrich A, Szczech E, Haertter S, Sharma AM, *et al.* Selective impairment in sympathetic vasomotor control with norepinephrine transporter inhibition. Circulation. 2003;107:2949-54.
11. Kamiya A, Kawada T, Yamamoto K, Michikami D, Ariumi H, Miyamoto T, *et al.* Muscle sympathetic nerve activity averaged over 1 minute parallels renal and cardiac sympathetic nerve activity in response to a forced baroreceptor pressure change. Circulation. 2005;112:384-6.
12. Kamiya A, Kawada T, Yamamoto K, Michikami D, Ariumi H, Miyamoto T, *et al.* Dynamic and static baroreflex control of muscle sympathetic nerve activity (SNA) parallels that of renal and cardiac SNA during physiological change in pressure. Am J Physiol Heart Circ Physiol. 2005;289:H2641-8.
13. Sundlof G, Wallin BG. Human muscle nerve sympathetic activity at rest. Relationship to blood pressure and age. J Physiol (Lond). 1978;274:621-37.
14. Nakamura T, Kawahara K, Kusunoki M, Feng Z. Microneurography in anesthetized rats for the measurement of sympathetic nerve activity in the sciatic nerve. J Neurosci Methods. 2003;131:35-9.
15. Kawada T, Shishido T, Inagaki M, Tatewaki T, Zheng C, Yanagiya Y, *et al.* Differential dynamic baroreflex regulation of cardiac and renal sympathetic nerve activities. Am J Physiol Heart Circ Physiol. 2001;280:H1581-90.
16. Kent BB, Drane JW, Blumenstein B, Manning JW. A mathematical model to assess changes in the baroreceptor reflex. Cardiology. 1972;57:295-310.
17. Marmarelis PZ, Marmarelis VZ. The whilte noise method in system identification. In: Analysis of Physiological Systems. New York: Plenum; 1978. p. 131-221.
18. Bendat JS, Piersol AG. Random data: analysis and measurement procedures. third edition. Canada: A Wiley-Interscience, 2000.
19. Glantz SA. Primer of biostatistics (4th ed.). New York: McGraw-Hill; 1997.
20. Ikeda Y, Kawada T, Sugimachi M, Kawaguchi O, Shishido T, Sato T, *et al.* Neural arc of baroreflex optimizes dynamic pressure regulation in achieving both stability and quickness. Am J Physiol. 1996;271:H882-90.
21. Habler HJ, Bartsch T, Janig W. Two distinct mechanisms generate the respiratory modulation in fibre activity of the rat cervical sympathetic trunk. J Auton Nerv Syst. 1996;61:116-22.
22. Morrison SF. Respiratory modulation of sympathetic nerve activity: effect of MK-801. Am J Physiol. 1996;270:R645-51.
23. Zhong S, Zhou SY, Gebber GL, Barman SM. Coupled oscillators account for the slow rhythms in sympathetic nerve discharge and phrenic nerve activity. Am J Physiol. 1997;272:R1314-24.
24. Iriki M, Dorward P, Korner PI. Baroreflex "resetting" by arterial hypoxia in the renal and cardiac sympathetic nerves of the rabbit. Pflugers Arch. 1977;370:1-7.
25. Hirai T, Musch TI, Morgan DA, Kregel KC, Claassen DE, Pickar JG, *et al.* Differential sympathetic nerve responses to nitric oxide synthase inhibition in anesthetized rats. Am J Physiol. 1995;269:R807-13.
26. Weiss ML, Claassen DE, Hirai T, Kenney MJ. Nonuniform sympathetic nerve responses to intravenous hypertonic saline infusion. J Auton Nerv Syst. 1996;57:109-15.
27. Macefield VG, Rundqvist B, Sverrisdottir YB, Wallin BG, Elam M. Firing properties of single muscle vasoconstrictor neurons in the sympathoexcitation associated with congestive heart failure. Circulation. 1999;100:1708-13.

28. Narkiewicz K, van de Borne PJ, Pesek CA, Dyken ME, Montano N, Somers VK. Selective potentiation of peripheral chemoreflex sensitivity in obstructive sleep apnea. Circulation. 1999;99:1183-9.
29. Kenney MJ, Barman SM, Gebber GL, Zhong S. Differential relationships among discharges of postganglionic sympathetic nerves. Am J Physiol. 1991;260:R1159-67.
30. Kenney MJ. Frequency characteristics of sympathetic nerve discharge in anesthetized rats. Am J Physiol. 1994;267:R830-40.
31. Kenney MJ, Weiss ML, Patel KP, Wang Y, Fels RJ. Paraventricular nucleus bicuculline alters frequency components of sympathetic nerve discharge bursts. Am J Physiol Heart Circ Physiol. 2001;281:H1233-41.
32. Eckberg DL. The human respiratory gate. J Physiol. 2003;548:339-52.
33. Kamiya A, Hayano J, Kawada T, Michikami D, Yamamoto K, Ariumi H, *et al.* Low-frequency oscillation of sympathetic nerve activity decreases during development of tilt-induced syncope preceding sympathetic withdrawal and bradycardia. Am J Physiol Heart Circ Physiol. 2005;289:H1758-69.
34. Furlan R, Porta A, Costa F, Tank J, Baker L, Schiavi R, *et al.* Oscillatory patterns in sympathetic neural discharge and cardiovascular variables during orthostatic stimulus. Circulation. 2000;101:886-92.
35. Van De Borne P, Montano N, Narkiewicz K, Degaute JP, Malliani A, Pagani M, *et al.* Importance of ventilation in modulating interaction between sympathetic drive and cardiovascular variability. Am J Physiol Heart Circ Physiol. 2001;280:H722-9.
36. Barman SM, Gebber GL. "Rapid" rhythmic discharges of sympathetic nerves: sources, mechanisms of generation, and physiological relevance. J Biol Rhythms. 2000;15:365-79.
37. Barman SM, Gebber GL, Zhong S. The 10-Hz rhythm in sympathetic nerve discharge. Am J Physiol. 1992;262:R1006-14.

REGULAR PAPER

J. Physiol. Sci. Vol. 56, No. 3; Jun. 2006; pp. 235–245
Online Jul. 7, 2006; **doi:10.2170/physiolsci.RP006006**

Sympathetic Neural Regulation of Heart Rate Is Robust against High Plasma Catecholamines

Toru KAWADA[1], Tadayoshi MIYAMOTO[1,2], Yuichiro MIYOSHI[1], Sayo YAMAGUCHI[1], Yukiko TANABE[1], Atsunori KAMIYA[1], Toshiaki SHISHIDO[1], and Masaru SUGIMACHI[1]

[1]Department of Cardiovascular Dynamics, Advanced Medical Engineering Center, National Cardiovascular Center Research Institute, Osaka, 565-8565 Japan; and [2]Japan Association for the Advancement of Medical Equipment, Tokyo, 113-0033 Japan

Abstract: The sympathetic regulation of heart rate (HR) may be attained by neural and humoral factors. With respect to the humoral factor, plasma noradrenaline (NA) and adrenaline (Adr) can reportedly increase to levels approximately 10 times higher than resting level during severe exercise. Whether such high plasma NA or Adr interfered with the sympathetic neural regulation of HR remained unknown. We estimated the transfer function from cardiac sympathetic nerve stimulation (SNS) to HR in anesthetized and vagotomized rabbits. An intravenous administration of NA (n = 6) at 1 and 10 $\mu g \cdot kg^{-1} \cdot h^{-1}$ increased plasma NA concentration (pg/ml) from a baseline level of 438 ± 117 (mean ± SE) to 974 ± 106 and 6,830 ± 917 ($P < 0.01$), respectively. The dynamic gain (bpm/Hz) of the transfer function did not change significantly (from 7.6 ± 1.2 to 7.5 ± 1.1 and 8.1 ± 1.1), whereas mean HR (in bpm) during SNS slightly increased from 280 ± 24 to 289 ± 22 ($P < 0.01$) and 288 ± 22 ($P < 0.01$). The intravenous administration of Adr (n = 6) at 1 and 10 $\mu g \cdot kg^{-1} \cdot h^{-1}$ increased plasma Adr concentration (pg/ml) from a baseline level of 257 ± 86 to 659 ± 172 and 2,760 ± 590 ($P < 0.01$), respectively. Neither the dynamic gain (from 8.0 ± 0.6 to 8.4 ± 0.8 and 8.2 ± 1.0) nor the mean HR during SNS (from 274 ± 13 to 275 ± 13 and 274 ± 13) changed significantly. In contrast, the intravenous administration of isoproterenol (n = 6) at 10 $\mu g \cdot kg^{-1} \cdot h^{-1}$ significantly increased mean HR during SNS (from 278 ± 11 to 293 ± 9, $P < 0.01$) and blunted the transfer gain value at 0.0078 Hz (from 5.9 ± 1.0 to 1.0 ± 0.4, $P < 0.01$). In conclusion, high plasma NA or Adr hardly affected the dynamic sympathetic neural regulation of HR.

Key words: systems analysis, neuro-humoral interaction, noradrenaline, adrenaline, isoproterenol.

The sympathetic regulation of heart rate (HR) may be attained by neural and humoral factors. One unique feature of the neural regulation, which is in contrast to the humoral regulation, is its quickness. The quickness of regulation may be best quantified by identifying dynamic characteristics of the input-output or stimulus-response relationship of a given system [1, 2]. Although we have identified the dynamic characteristics of the HR regulation by the cardiac sympathetic nerve by using a transfer function analysis [3, 4], we ignored the possible effects of plasma catecholamines on the transfer function. Plasma concentrations of noradrenaline (NA) and adrenaline (Adr) can increase during systemic sympathetic activation. For instance, plasma NA and Adr both increase to approximately 10 times their respective resting levels during severe exercise [5]. They increase to approximately 6 and 20 times, respectively, during acute myocardial infarction [5]. Whether such high plasma NA or Adr interfered with the dynamic sympathetic neural regulation of HR remained unanswered.

Two mutually opposing hypotheses can be put forward regarding interactions between the humoral and neural factors in the sympathetic regulation of HR. The activation of presynaptic (or prejunctional) α_2-adrenergic receptors located on the postganglionic sympathetic nerve terminals inhibits NA release [6], which would result in the attenuated HR response to cardiac sympathetic nerve stimulation (SNS). In contrast, the activation of presynaptic (or prejunctional) β_2-adrenergic receptors located on the postganglionic sympathetic nerve terminals facilitates NA release [7], which would result in the augmented HR response to cardiac SNS. Besides these interactions, high plasma NA can increase the cardiac uptake of NA [8], which would modify the HR response to cardiac SNS.

The aim of the present study was to test the hypothesis that high plasma NA or Adr alters the dynamic sympathetic neural regulation of HR. Using anesthetized rabbits, we examined the HR response to random cardiac SNS under the condition of elevated plasma NA or Adr induced by exogenous administration. We also examined the effects of an intravenous administration of a β-adrenergic agonist isoproterenol on the HR response to SNS. The results of

Received on Jun 1, 2006; accepted on Jul 4, 2006; released online on Jul 7, 2006; doi:10.2170/physiolsci.RP006006
Correspondence should be addressed to: Toru Kawada, Department of Cardiovascular Dynamics, Advanced Medical Engineering Center, National Cardiovascular Center Research Institute, 5-7-1 Fujishirodai, Suita, Osaka, 565-8565 Japan. Phone: +81-6-6833-5012 (Ext. 2427), Fax: +81-6-6835-5403, E-mail: torukawa@res.ncvc.go.jp